JOURNAL OF GEOPHYSICAL RESEARCH, VOL. 113, C11010, doi:10.1029/2007JC004720, 2008

A numerical study of the Southwestern Atlantic Shelf circulation: Stratified ocean response to local and offshore forcing

Elbio D. Palma,[1,2] Ricardo P. Matano,[3] and Alberto R. Piola[4,5,6]

Received 3 January 2008; revised 12 May 2008; accepted 16 July 2008; published 11 November 2008.

[1] This article discusses the results of a suite of numerical simulations of the oceanic circulation in the Southwestern Atlantic Shelf region that are aimed to characterize its mean circulation and seasonal variability and to determine the dynamical mechanisms controlling them. Our experiments indicate that south of 40°S the mean circulation is dominated by a general northeastward flow in the southern portion of the shelf, which is controlled by the discharges from the Magellan Straits, tidal mixing, wind forcing, and the offshore influence of the Malvinas Current farther north. The region from 40°S to 33°S presents the highest seasonal variability, with intrusions of cold sub-Antarctic waters and the northward expansion of mixtures of the Río de la Plata waters in late fall and a slower retraction of the plume during spring-summer. Wind stress variability seems to be the primarily forcing mechanism for the plume dynamics. These model results are in reasonable agreement with observations and previous model results. The present solutions also reveal important additional features of the shelf response. The along-shelf circulation, for example, is largely driven by the western boundary currents in the middle and outer shelf, with induced transports that are 3 times larger than in experiments forced by winds and tides. The analysis also indicates that the upstream influence of the Malvinas Current is felt well beyond its retroflection point in the form of a northward middle-shelf current and that the interaction of the Brazil Current with the Brazilian shelf topography is primarily responsible for inducing steady shelf break upwelling.

Citation: Palma, E. D., R. P. Matano, and A. R. Piola (2008), A numerical study of the Southwestern Atlantic Shelf circulation: Stratified ocean response to local and offshore forcing, *J. Geophys. Res.*, *113*, C11010, doi:10.1029/2007JC004720.

1. Introduction

[2] The Southwestern Atlantic Shelf (SWAS) extends from the tip of Tierra del Fuego (55°S), Argentina to Cabo Frío (~22°S), Brazil. This is the largest continental shelf of the southern hemisphere, and one of the most biologically productive areas of the world ocean [*Bisbal*, 1995; *Acha et al.*, 2004]. The SWAS is very wide in the south (~850 km) but narrows markedly toward the north. Its general circulation patterns consist of a northeastward flow from the tip of Patagonia to the mouth of the La Plata River, and a southwestward flow farther north (Figure 1). The shelf circulation is driven by strong tides [*Glorioso and Flather*, 1997; *Palma et al.*, 2004a], large freshwater discharges [*Piola et al.*, 2005], highly variable winds [*Palma et al.*, 2004b], and the influence of two distinctive western boundary currents: the Brazil and Malvinas currents [*Piola and Matano*, 2001].

[3] In spite of its ecological and economical importance [*Costanza et al.*, 1997] our knowledge of the circulation patterns over this vast region is limited by the scarcity of observations. To the best of our knowledge, for example, there are only three documented descriptions of current meter time series, none of which lasted longer than a few months [*Rivas*, 1997; *Zavialov et al.*, 2002; *Castro and de Miranda*, 1998], and only one description of drifter trajectories [*de Souza and Robinson*, 2004]. Regional circulation patterns have been indirectly inferred from hydrographic observations and from a relatively small number of regional simulations [*Forbes and Garraffo*, 1988; *Glorioso and Flather*, 1995; *Rivas and Langer*, 1996; *Pereira*, 1989; *Zavialov et al.*, 1999; *Campos et al.*, 2000; *Castelao et al.*, 2004]. In this article we aim to improve these descriptions through the analysis of a suite of long-term numerical simulations that, for the first time, considers the interactions between the shelf and the deep ocean and includes all the major forcings on the SWAS circulation, namely: winds, tides, freshwater discharges, and western boundary currents. Our objectives are to characterize the annual mean circula-

[1] Departamento de Física, Universidad Nacional del Sur, Bahía Blanca, Argentina.
[2] Also at Instituto Argentino de Oceanografía, Consejo Nacional de Investigaciones Científicas y Técnicas, Bahía Blanca, Argentina.
[3] College of Oceanic and Atmospheric Sciences, Oregon State University, Corvallis, Oregon, USA.
[4] Departamento Oceanografía, Servicio de Hidrografía Naval, Buenos Aires, Argentina.
[5] Also at Departamento de Ciencias de la Atmósfera y los Océanos, Universidad Nacional de Buenos Aires, Buenos Aires, Argentina.
[6] Also at Consejo Nacional de Investigaciones Científicas y Técnicas, Buenos Aires, Argentina.

0148-0227/08/2007JC004720$09.00

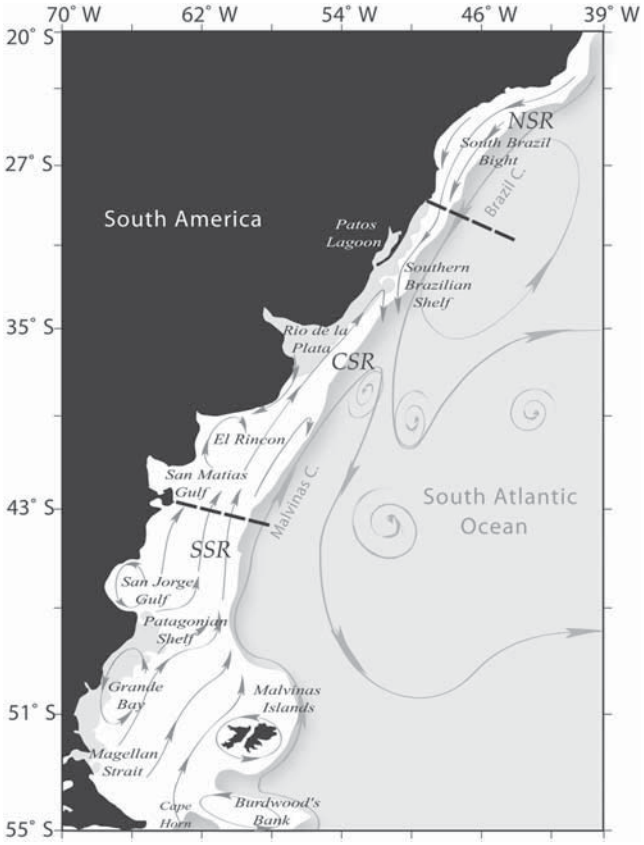

Figure 1. Map showing the geographical locations referred to in the text. Curved light lines indicate the schematic shelf circulation inferred from hydrographic observations and previous models. Heavy gray lines indicate the schematic path of the offshore boundary currents. Heavy dashed black lines indicate the approximate boundaries of the shelf partition used in the discussion of model results (Southern Shelf Region (SSR), Central Shelf Region (CSR), and Northern Shelf Region (NSR)).

tion and its seasonal variability and to determine the dynamical mechanisms controlling them.

[4] This paper has been organized as follows, after this introduction, in Section 2 we offer a brief review of previous observational and numerical studies of the shelf circulation. Section 3 contains a short description of the 3-D circulation model, the procedure for estimating the forcing fields and the set-up of the different numerical experiments. Section 4 describes the model results. It starts with a brief discussion of the offshore circulation and it is followed with an in-depth analysis of shelf circulation and its sensitivity to different forcing mechanisms. Finally, section 5 summarizes and discusses all the previous results.

2. Background

[5] For the purposes of description the SWAS can be divided in three distinctive regions: the Southern Shelf Region (SSR), extending from the tip of the continent to 41°S, the Central Shelf Region (CSR), extending from 41°S to 28°S, and the Northern Shelf Region (NSR), extending from 28°S to 22°S. Although the precise limits of these regions are arbitrary, each of them has unique characteristics that distinguish them from the other ones. The SSR, which is also known as Patagonian Shelf, is the widest portion of the southwestern Atlantic Shelf, it is characterized by high tidal amplitudes, the low-salinity discharges from the Magellan Straits, strong and persistent westerly winds (with small seasonal variations), and the offshore influence of the Malvinas Current. The CSR is distinguished by the freshwater discharges from the Río de la Plata (Plata hereafter) and the Patos Lagoon, relatively weak and seasonally reversing winds, and the offshore influence of the Brazil/Malvinas Confluence. The NSR is a narrow shelf with strong density stratification, small tidal amplitudes, prevailing northwesterly (alongshore) winds, and the offshore influence of the Brazil Current. In what follows we will offer a succinct description of each of these regions.

2.1. SSR

[6] The hydrographic structure of this region has been extensively described in previous studies [e.g., *Guerrero and Piola*, 1997; *Bianchi et al.*, 2005]. The outer-shelf water mass is characterized as Sub-Antarctic Shelf Water, a relatively fresh ($S < 34$) variety of sub-Antarctic water that is injected onto the SSR through the Le Maire Strait, the Cape Horn and possibly the shelf break (i.e., Malvinas Current). In the middle and inner shelf there is a distinct low-salinity surface tongue ($S < 33.4$) that is associated with the discharges from the Magellan Strait [*Bianchi et al.*, 2005] (Figure 2b).

[7] The SSR harbors some of the largest tidal amplitudes in the world ocean [*Panella et al.*, 1991]. The tidal wave enters through the southern boundary and propagates to the north. Tidal motions in the middle and inner shelf are dominated by the semidiurnal harmonic (M_2) and in the outer shelf by the diurnal (K_1) and semidiurnal harmonics [*Glorioso and Flather*, 1997; *Palma et al.*, 2004a]. Tidal forcing is particularly important in the inner-shelf region where it accounts for more than 90% of the total kinetic energy variance [*Rivas*, 1997].

[8] Although the SSR is within the "*roaring forties*" beltway little is known about the wind driven circulation in this region. *Forbes and Garraffo* [1988] estimated along shelf surface currents of $\sim$20 cm s^{-1} using a simple Ekman-type model. *Glorioso and Flather* [1995] and *Palma et al.* [2004a, 2004b] postulated the existence of a broad northeastward flow with counterclockwise gyres within the Grande Bay and the San Jorge Gulf. None of these features, however, have been confirmed by direct observations, although *Rivas* [1994] and *Rivas and Langer* [1996] postulated the existence of an along shelf flow with a depth-averaged speed of 4 cm s^{-1}.

2.2. CSR

[9] The hydrographic structure of the CSR is characterized by two water masses, Sub-Antarctic Shelf Waters ($S < 34$) in the south and Subtropical Shelf Water ($S > 34.5$) in the north [*Piola et al.*, 2000] (Figure 2b). These water masses reflect the dominant circulation patterns of the region. In the southern portion of the CSR there is a northeastward inflow of high-salinity waters during the fall and winter, and a southward inflow of low-salinity waters from the La Plata River during the spring and summer

[*Lucas et al.*, 2005]. In the northern portion there is a southward flow that weakens during the winter [*Zavialov et al.*, 2002]. The Sub-Antarctic and Subtropical Shelf Waters are separated by the Subtropical Shelf Front, a density compensated salinity and temperature front located near 32°S [*Piola et al.*, 2000]. The tidal amplitudes in the CSR are relatively small [*Palma et al.*, 2004a], and the wind stress forcing is characterized by weak intensities (~0.05 Pa) and large seasonal variations [*Palma et al.*, 2004b]. *Palma et al.* [2004a] on the basis of results from a three dimensional numerical model postulated that there is a seasonal reversal of the circulation, but this hypothesis has not been confirmed by observations.

2.3. NSR

[10] The water mass structure of the NSR is dominated by warm and salty Tropical Water (T > 20°C, S > 36.40) in the surface (Figure 2b) and cold and relatively fresh South Atlantic Central Water below 200 m [*Castro and de Miranda*, 1998]. The wind direction in this region is predominantly from the northeast (i.e., upwelling favorable), except during the passage of cold fronts in the austral winter [*Campos et al.*, 1995]. Tidal amplitudes in the NSR are low (<40 cm), with a dominance of the semidiurnal component [*Harari and de Camargo*, 2003; *Castro and de Miranda*, 1998; *Palma et al.*, 2004a]. Scant direct current observations indicate the existence of a seasonally varying along-shelf flow in the inner shelf and a mean southwestward flow of in the middle and outer shelf [*Castro and de Miranda*, 1998]. Numerical simulations indicate that there is a southwestward flow that intensifies during the spring and summer and weakens toward the fall [*Palma et al.*, 2004a]. They also indicate that the poleward advection of eddies by the Brazil Current generates shelf break upwelling [*Campos et al.*, 2000; *Castelao et al.*, 2004].

3. Model Description

[11] The numerical model used in this study is the Princeton Ocean Model [*Blumberg and Mellor*, 1987]. The model uses a curvilinear grid that extends from 55°S to 18°S and from 70°W to 40°W with a horizontal resolution of 5 km near the coast and 20 km near the eastern boundary (Figure 1). The bathymetry was interpolated from data of the Argentinean Navy supplemented with the *Smith and Sandwell* [1997] database for depths greater than 200 m. The vertical resolution comprises 25 vertical sigma levels with higher resolution in the top and bottom boundary layers. The model has three open boundaries were a combination of radiation and advection boundary conditions is used [*Palma and Matano*, 2000]. Further details about the grid configuration can be found in the paper by *Palma et al.* [2004a].

[12] The model was forced with data extracted from global models and databases. Tidal amplitudes and phases were interpolated from *Egbert et al.*'s [1994] model, and boundary inflows form the POCM-4 eddy-permitting global ocean model [*Tokmakian and Challenor*, 1999]. At the surface the model was forced with wind stress data from the ECMWF reanalysis [*Trenberth et al.*, 1990]. Heat and freshwater fluxes were parameterized with a Newtonian damping to observed sea surface temperature (SST) and salinity (SSS). Climatological SST data was extracted from satellite observations [*Casey and Cornillon*, 1999] while the SSS climatology was constructed from seasonal quality-controlled historical hydrographic data. Climatological freshwater discharges obtained from direct measurements are injected at the La Plata River mouth (23,000 $m^3\ s^{-1}$ on average) and Patos Lagoon (2000 $m^3\ s^{-1}$) [*Piola et al.*, 2008a]. The Magellan Strait outflow, estimated from a high-resolution numerical model of the Magellan Strait forced by tides, wind forcing and interoceanic sea level differences was set to 85,000 $m^3\ s^{-1}$.

[13] After a 6-year run initialized with annual mean temperature and salinity extracted from a World Atlas [*Levitus and Boyer*, 1994; *Levitus et al.*, 1994] and annual mean forcing, the model was run for another 6 years with monthly forcing, in which period we saved in the last 3 years 3 day averages for analysis. Additional numerical experiments were designed to investigate the relative importance of various dynamical mechanisms that sustains the mean circulation and its seasonal variability. Six different model scenarios are used to isolate the predominant mechanisms: (1) the benchmark experiment with full forcing (EXP1); (2) a baroclinic experiment initialized as in EXP1 but without tides, winds, and freshwater forcing (EXP2); (3) a baroclinic experiment initialized with a homogeneous ocean and forced with freshwater discharges (EXP3); (4) the same set-up as EXP3 but with the inclusion of tidal forcing (EXP4); (5) a barotropic experiment forced with climatological winds and tides (EXP5); and (6) a barotropic ocean forced with climatological winds (EXP6). The last two experiments were described in detail by *Palma et al.* [2004a]. Table 1 summarizes the general characteristics of all the experiments discussed in this article.

4. Results

4.1. Offshore Circulation

[14] The offshore circulation has a strong influence on the shelf dynamics therefore in this section we will briefly compare the model results in this region with observations. The offshore circulation patterns generated by the model are in good agreement with observations (Figure 2a). The Brazil/Malvinas Confluence (BMC), for example, is located at its observed latitude of 38°S [*Olson et al.*, 1988; *Matano et al.*, 1993; *Garzoli and Giulivi*, 1994]. The model's skill to reproduce such a well-known feature of the regional circulation is particularly noteworthy since global, eddy-permitting models (i.e., the Parallel Ocean Circulation Model) have the confluence located several degrees southward of where it should be [*Fetter and Matano*, 2008]. The deficiency of the global models can be attributed to their lack of resolution of the bottom topography, which is known to be a critical element in the formation of the Malvinas Current (MC) and, hence, in the determination of the location of the confluence [*Matano*, 1993]. The transport of the Brazil Current (BC) in the model increases from 8.5 Sv (1 Sv = $10^6\ m^3\ s^{-1}$) at 25°S to nearly 33 Sv at 36°S (Figure 2a). Transport values between 5 Sv and 10 Sv have been computed in the upper 500 m of the BC around 24°S using geostrophic methods [*Stramma*, 1989]. As the BC flows southward, its flow intensifies by about 5% per 100 km, which is similar to the growth rate in the Gulf

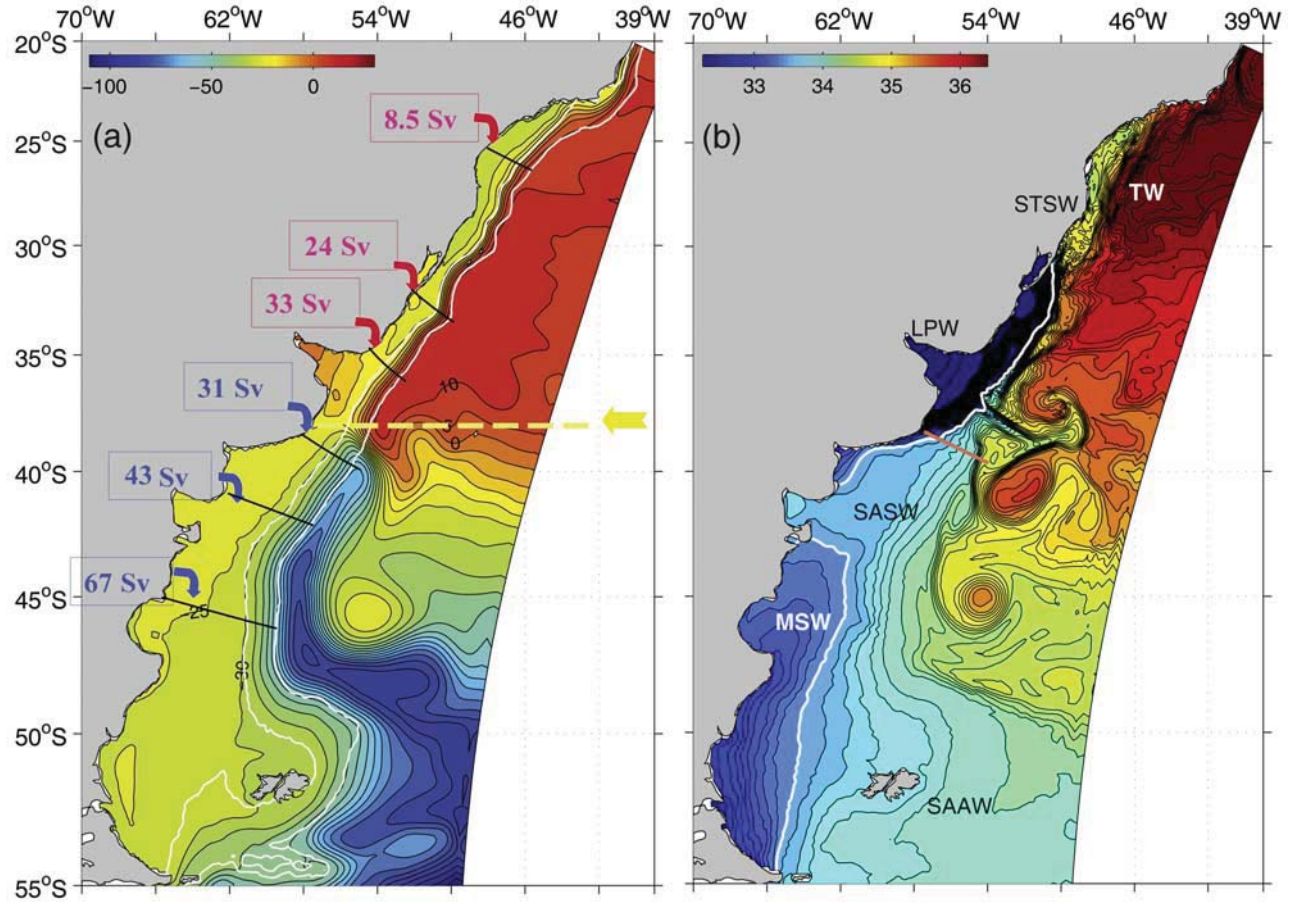

Figure 2. (a) Climatological annual mean sea surface height (SSH) derived from EXP1. CI = 5 cm. Numbers inside boxes indicate transport (in Sv) through each cross section. The dashed yellow line indicates the mean position of the Brazil/Malvinas Confluence. The white lines indicate the 200 m and 1000 m isobaths (b) Snapshot of sea surface salinity obtained from the model (EXP1). Main water masses shown are as follows: Magellan Strait Water (MSW), Sub-Antarctic Shelf Water (SASW), Subtropical Shelf Water (STSW), La Plata Water (LPW), Sub-Antarctic Water (SAAW), and Tropical Water (TW). The white line indicates the 33.5 psu contour. Note the intrusion of low-salinity waters at the confluence and the shedding of high-salinity anticyclonic eddies from the Brazil Current. The red line is the cross section illustrated in Figure 5.

Stream, although transport values in the BC are considerably less [*Peterson and Stramma*, 1991]. Thus, at about 33°S the total geostrophic transport (which includes a recirculation cell in the upper 1400 m) is about 18 Sv, and reaches values of more than 22 Sv at about 38°S, where it encounters the MC [*Gordon and Greengrove*, 1986; *Peterson and Stramma*, 1991]. The transport of the MC in the model decreases downstream from 67 Sv at 45°S to 43 Sv at 42°S, reaching 31 Sv at 39°S. Estimates of the volume transport of the MC vary widely in the literature, ranging from 10 Sv to 70 Sv, although several recent studies converge toward 40–50 Sv at 41°S. *Gordon and Greengrove* [1986] using hydrographic sections and assuming a level of no motion at 1400 m estimated the MC transport at about 10 Sv at 42°S. Alternatively, using the same data set, *Peterson* [1992] found 60 Sv in the upper 2000 m at 42°S and 75 Sv in total, while at 46°S he found 70 Sv in the upper 2000 m and 88 Sv in total. His estimates were based on mass balance constrained by bottom velocities and were therefore the first including a barotropic contribution to the flow. *Peterson et al.* [1996] also found 73 Sv at 42°S by combining hydrographic data and Lagrangian drifter velocities. Using ADCP and hydrographic measurements *Saunders and King* [1995] estimated a transport of 50 Sv at 45°S. Combining 18 months of current meter

Table 1. General Description of the Numerical Experiments[a]

Experiment Number	Tides	Winds	Malvinas Current and Brazil Current	Freshwater	Initial Condition
1	yes	yes	yes	yes	stratified
2	no	no	yes	no	stratified
3	no	no	no	yes	homogeneous
4	yes	no	no	yes	homogeneous
5	yes	yes	no	no	homogeneous
6	no	yes	no	no	homogeneous

[a]EXP5 and EXP6 were described in detail by *Palma et al.* [2004a, 2004b]. Freshwater forcing includes Magellan Strait (~85,000 m^3 s^{-1}), La Plata River (~23,000 m^3 s^{-1}), and Patos Lagoon (~2000 m^3 s^{-1}) discharges.

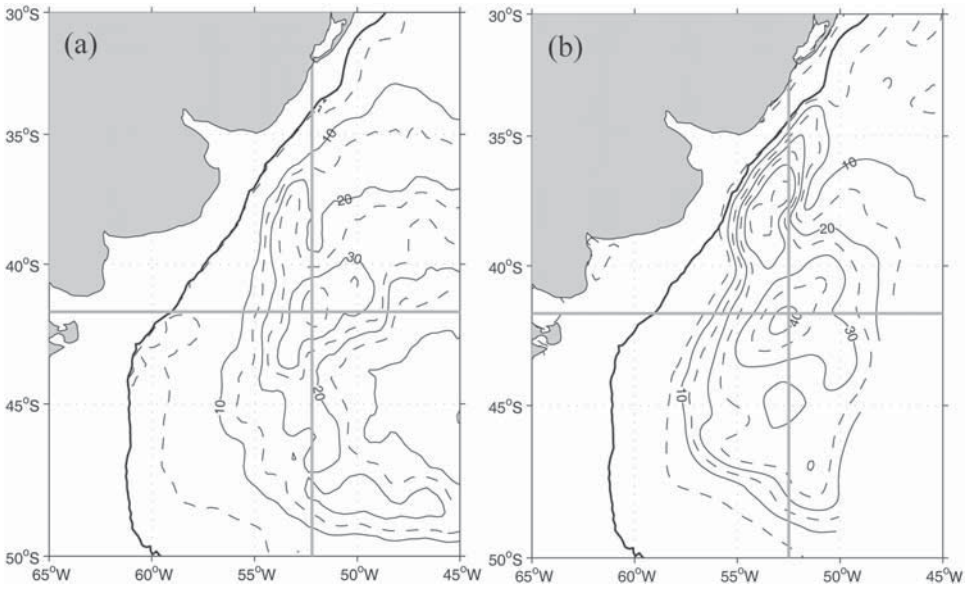

Figure 3. (a) RMS of SSH (cm) computed from altimetic tracks (Archiving, Validation, and Interpretation of Satellite Oceanographic data data set 1992–2006) and (b) RMS of SSH obtained from the model (EXP1). The bold black line shows the 200 m isobath. Note the maxima in RMS (>35 cm) centered close to 42°S, 52°W (gray lines) and the northward extension of maximum variability along the shelf break north of 38°S, both in the model and observations.

measurements across the MC between 40°S and 41°S and sea level satellite observations *Vivier and Provost* [1999] estimated a transport of 41.5 ± 12.2 Sv. *Vigan et al.* [2000] using an inverse model and surface temperature images have concluded that the transport of the MC decreases from south to north with an estimate of 25 ± 5 Sv between 40°S and 41°S. Thus, the model-derived transports appear to be in good qualitative agreement with observations.

[15] The BMC spawns one of the most spectacular eddy fields of the global ocean [*Piola and Matano*, 2001]. The sea surface temperature and surface salinity anomalies of these rings can be as large as 10°C and 2 psu and therefore are an important mechanism for the meridional transfer of salt and heat. Figure 2b illustrates the model capability to generate the high internal variability of the BMC through a snapshot of SSS. Figure 2b captures the instant when an intrusion eddy is clearly visible near 45°S, 54°W while a second eddy is close to detachment further north. The size and vertical structure of the eddies (not shown) are in good agreement with those computed from hydrographic observations. Also shown in Figure 2b is a large-scale filament of low-salinity waters expelled from the shelf that after meandering intrudes into the high-salinity tropical waters. To quantify the model skill to reproduce the mesoscale variability of this region we computed the SSH variances from all the available satellite altimeter data up-to-date (Archiving, Validation, and Interpretation of Satellite Oceanographic data data set, 1992–2006) (Figure 3a). Comparing the observed and modeled variability we note the following similarities and differences. There is a well defined maximum (>35 cm) centered at approximately 42°S, 52°W both in the model and the observations. North of 38°S the model shows a region of maximum variability extending along the shelf break. The observed data set shows a similar feature extending northward of 38°S, although the intensity and meridional extent in the observations is smaller than in the model. Part of the discrepancy could be attributed to the data processing (gridding of along-track sampling might smooth sharp peaks), and limitations of the satellite retrieval in shallower areas (depths shallower than 1000 m are excluded to avoid tidal contamination). The general pattern of eddy variability, however, is retained. Near the model open eastern boundary the modeled variability is smaller than observed, a fact that reflects the zonal limitation of the present model to properly simulate the offshore extension of the BMC eddy variability.

[16] To further evaluate the model's realism we compared the surface velocities from the model (at 15 m depth) with values derived from drifter data collected by the Global Drifter Center of NOAA's Atlantic Oceanographic and Meteorological Laboratory (Figure 4). The drifter velocities are computed on the basis of all available observations in regions of 0.5° latitude × 0.5° longitude. The observations and model results show coherent jets, with maximum surface speeds of 0.4 m s^{-1}, along the MC axis and larger than 0.8 m s^{-1} in the southward jet near the BMC. The overall current structure across the MC: the large cross-isobath increase in current magnitude toward the shelf break, the maximum core velocity and the subsequent inversion in velocity direction (the retroflection) shown in the observations is well resolved by the model (Figures 4c and 4d). At 50°S between 55°W and 60°W both drifter data and modeled currents shows northwestward flow. Along 60°W the drifters and the modeled velocities show northward flow along the isobaths. North of 40°S, the modeled northeastward flow in the continental shelf extends up to 34°S, closely following the drifter's behavior. Along the continental slope of Brazil and the MC return the model

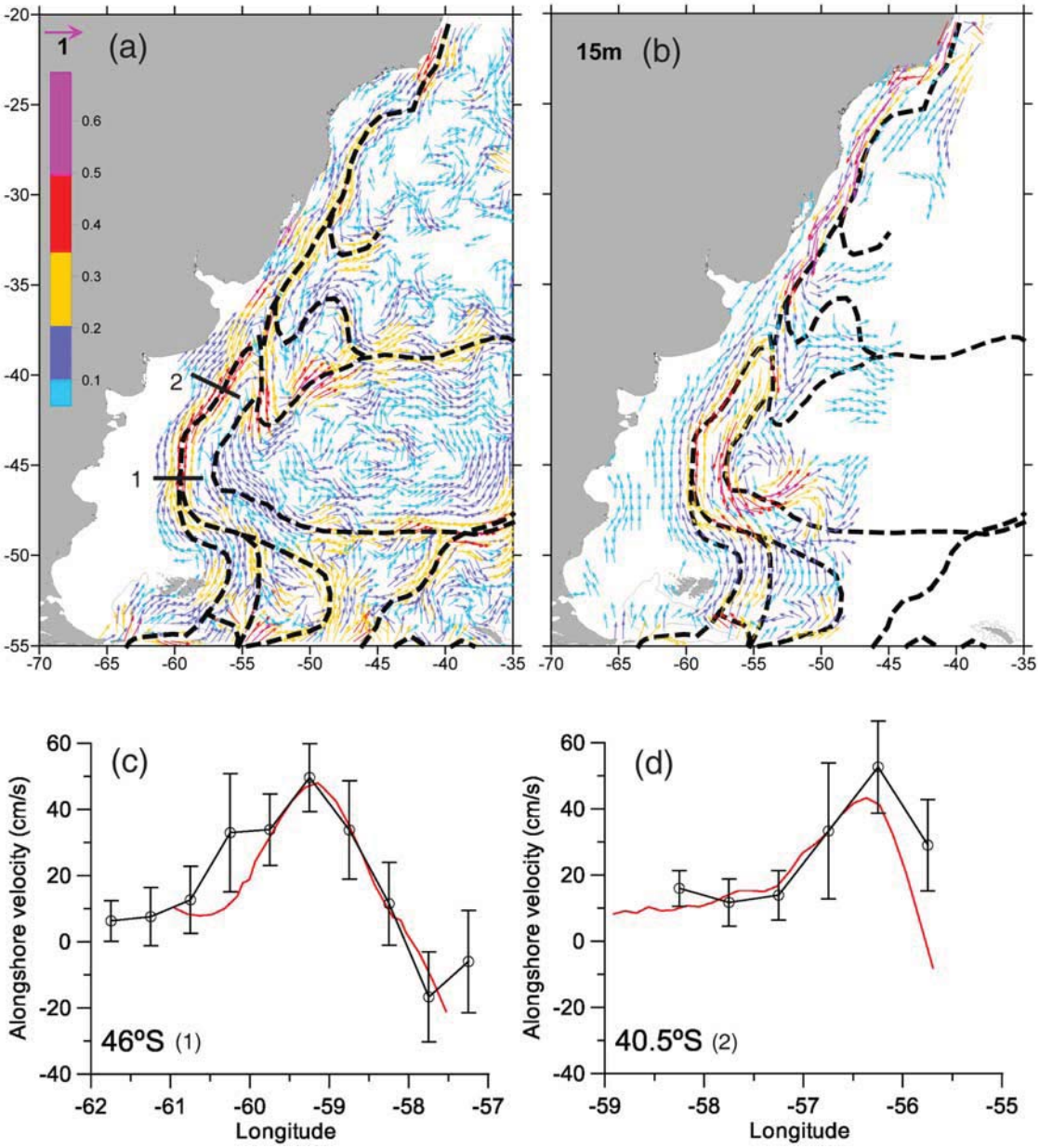

Figure 4. (a) Annual mean sea surface velocity in the SW Atlantic computed from 10 years (1989–2001) of surface drifters. Only vectors with surface speed greater than 5 cm s^{-1} are shown, and vectors are color scaled. Coherent high-velocity jets are indicated by the dashed lines. (b) Surface velocity (15 m depth) obtained from the model (EXP1). Along-isobath velocity sections (c) 1 and (d) 2 indicated in Figure 4a, drifters (black line), and model results (red line). Vertical bars indicate standard deviation of the drifter-derived velocity about the mean.

shows similar patterns, but larger speeds. The model velocity field has also a weaker recirculation cell of the BC near 33°S (Figure 4b). These differences are relatively minor since the larger speeds in the model can be attributed to the smoothing of the drifter data, and the absence of a stronger recirculation cell due to the limited offshore extension of the model's domain.

[17] There is also good qualitative agreement between hydrographic cross sections taken from synoptic observations and the model results. Model and observations show a wedge of cold and fresh subpolar water separating the warm and salty subtropical water farther offshore (Figure 5). Since the numerical experiment is initialized with observations we also included in our comparison the temperature and salinity profiles on the basis of the *Levitus and Boyer* [1994] data used to initialize the model. Note the marked differences between the initial profiles (Figures 5a and 5d) and the final model results (panels b and e). These differences are created by the model dynamics, which are able to reshape the overly smooth Levitus and Boyer fields into a pattern that more closely resembles the observations (Figures 5c and 5f).

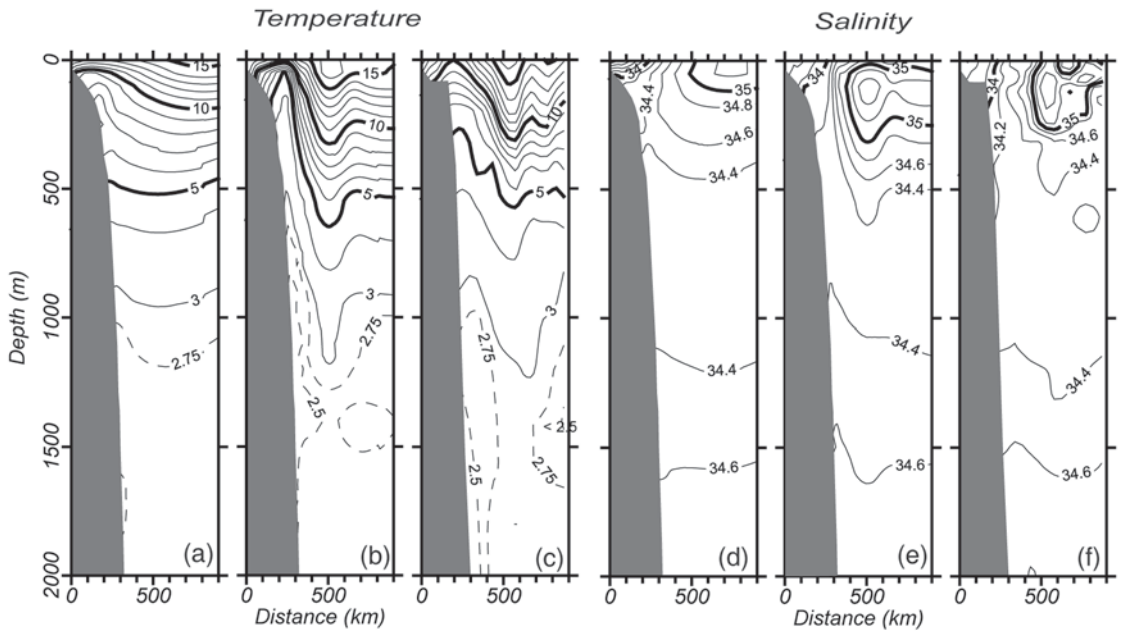

Figure 5. Vertical (a, b, c) temperature and (d, e, f) salinity cross sections of the upper 2000 m of the water column near 38°S (see Figure 2b). Figures 5a and 5d are the model initialization fields taken from a global database [*Levitus and Boyer*, 1994], Figures 5b and 5e show the results from the model-derived annual fields (EXP1), and Figures 5c and 5f are derived from synoptic hydrographic data.

4.2. Shelf Circulation

4.2.1. SSR (55°S to 41°S)

[18] The circulation in the SSR is forced by large tides, intense offshore winds and the barotropic pressure gradients generated by the Malvinas Current (MC). The surface salinity patterns generated by the model are dominated by the low-salinity plume from the Magellan Straits, which extends up to 40°S (Figure 6a). The depth-averaged circulation consists of a broad northeastward flow with average velocities of ~3.5 cm s^{-1} and peaks of more than 7 cm s^{-1}. (Figure 6b). The circulation intensifies in the outer shelf, where it is highly influenced by the MC. South of ~49°S there is a well-defined jet in the inner shelf, which is known as the Patagonian Current that juxtaposes the plume from the Magellan Straits [*Brandhorst and Castello*, 1971; *Bianchi et al.*, 2005; *Romero et al.*, 2006]. There are anticlockwise gyres within Grande Bay and San Jorge Gulf with weak, southward flowing depth-averaged coastal currents. The vertical structure of the circulation is roughly equivalent to a two-layer flow where the upper layer is directed toward the northeast and the bottom layer in the opposite direction (Figures 6c and 6d). A simple mass balance of the model results indicates that the surface Ekman layer exports water to the North and the East that is largely compensated by inflow from the South. Only a small part of the northeastward transport (less than 10% on average) is compensated by inshore flow beneath the surface layer, closing the mass balance. These results are in agreement with previous studies in that the cross-shelf circulation generated by cross-shelf wind stress (dominant in southern SSR) is significantly weaker than those produced by along-shelf winds of similar magnitude [*Greenberg et al.*, 1997]. The lower layer entrains waters from the deep ocean at the Le Maire Straits and to a lesser extent across the Malvinas shelf break front (Figure 6d) [*Matano and Palma*, 2008]. These inshore-directed subsurface currents generate areas of upwelling near the coast. However, because of the weak magnitude of the bottom currents, the associated vertical velocity is substantially less that in typical along-shelf upwelling winds. These weak upwelling velocities plus the efficient vertical homogenization of the water column associated with the large amplitude Patagonian tides [*Palma et al.*, 2004a] makes very difficult the detection of cold strips of upwelled water near the coast by means of SST. The quantitative comparison of annual-averaged surface model currents (within 20 m of the surface) with the available moored measurements indicates a good agreement, less than 10% error both in magnitude and direction (Figure 7 and Table 2). The largest difference in current magnitude (~25%) is found near the shelf break at site C. It should be noted however, that the mooring site is on average at shallower depth than in the model because of the unavoidable bathymetric smoothing in regions of very steep slopes like the shelf break and therefore, model points slightly inshore of point C have speeds closer to that observed. The magnitude and direction of the depth-mean horizontal circulation on the shelf generated by the model (Figure 6b) are qualitatively consistent with those inferred by *Rivas and Langer* [1996] using an inverse box-model on the basis of historical temperature observations and heat fluxes. Comparison of the along-shelf transports of that solution with the results shown in Figure 6b indicates only approximate agreement. The average along-shelf transport of the inverse model increases toward the north and is about 3 times larger than our model results. The origin of this difference can be attributed to the poor representation of the shelf break in the box model (1° resolution), which allowed a larger contribution

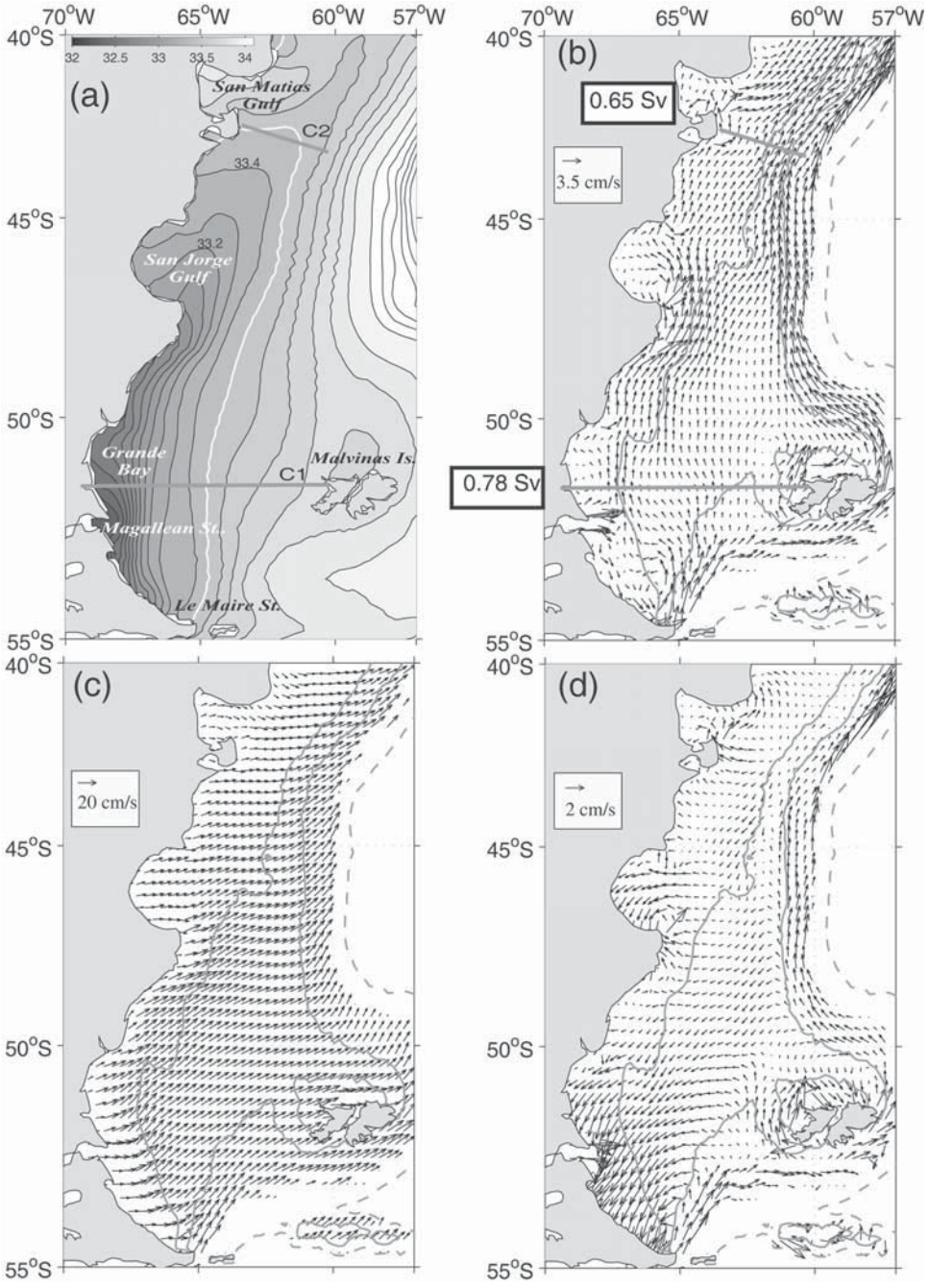

Figure 6. Annual mean circulation in the Southern Shelf Region from EXP1. (a) Sea surface salinity. The white line indicates the 33.5 isohaline. (b) Depth-averaged velocity vectors. Numbers inside boxes indicate the transport (in Sv) through the indicated cross section. (c) Surface velocity vectors. (d) Bottom layer velocity vectors. Solid gray lines indicate the 100 and 200 m isobaths; the dashed line is the 1000 m isobath. The vector fields are shown for depths less than 500 m.

of the MC to the along-shelf transport along the eastern boundary. The spatial structure of the model salinity distribution (Figure 6a) is in good agreement with historical hydrographic observations [*Bianchi et al.*, 2005].

[19] One of the most notorious characteristics of the SSR circulation is the development of the Patagonian Current (Figure 6b). Although this current is obviously linked to the discharges from the Magellan Straits, the mechanisms that control its path and volume transport are far from clear. Note, for example, that it does not flow along the coastline, as expected from a density driven flow, but instead follows the 100 m isobath (Figure 6a). To establish the dynamical mechanisms that control the Patagonian Current we did three ancillary experiments: EXP3, EXP4 and EXP5 (Table 1). EXP3 is forced with the discharge from the Magellan Straits only. EXP4 is forced with the discharges from the Magellan Straits and tidal forcing. EXP5 is a barotropic version of EXP1 that was forced with winds and

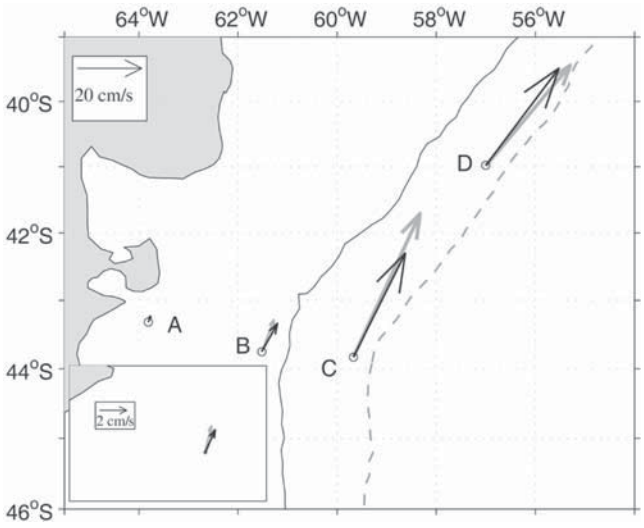

Figure 7. (top) Comparison of modeled and observed surface currents in the SSR, showing model velocities (black) and mooring measurements (gray). Points A and B are from *Rivas* [1997]. Points C and D are from Global Environmental Facility project measurements. (bottom) A zoom of the point A region. The 200 m (full line) and 1000 m isobaths (dashed line) are also shown.

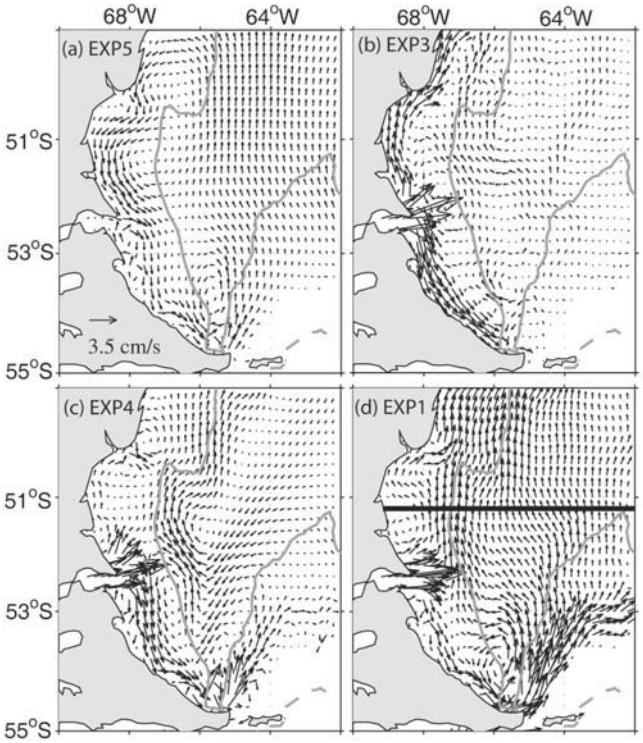

Figure 8. Depth-averaged circulation in Grande Bay. Results from (a) EXP5, (b) EXP3, (c) EXP4, and (d) EXP1. The gray line indicates the 100 m and 200 m isobaths, and the heavy black line in Figure 8d indicates the cross section where the momentum balance (Figure 9) is evaluated.

tides but lacks the influence of the western boundary currents and freshwater discharges (see the paper by *Palma et al.* [2004a] for an extensive description of this experiment). The comparison of the different experiments shows that the most contrasting results are between EXP5 and EXP3 (Figures 8a and 8b). In the former there is a coastally trapped current flowing southward along the shorelines of the Grande Bay. In the later the coastal current flows in the opposite direction. None of these experiments, however, is able to develop the Magellan Plume in its observed place [*Bianchi et al.*, 2005] (see also Figure 6a). In EXP4 however, the effects of tidal rectification move the freshwater discharge away from the coast, but now the core of the current is located offshore of the observed position (Figure 8c) and the plume does not have the spatial structure suggested by the observations [*Bianchi et al.*, 2005]. The shortcoming of EXP3 is corrected in EXP1, where the inclusion of the MC and wind stress forcing displace the jet axis close to the 100 m isobath and reinforces its frontal characteristics (Figure 8d).

[20] To quantify the dynamical processes just described we computed the depth-averaged cross-shelf momentum balance of the four experiments (Figure 9). The dominant terms of the steady state climatologically averaged momentum budget in the cross-shore direction are:

$$ADV_x - fv + g\eta_x + \Phi_x - (K_m u_z)_z = 0, \qquad (1)$$

where v is the alongshore velocity component ($-fv$ is the cross-shore Coriolis term), η_x is the barotropic pressure gradient, Φ_x is the baroclinic pressure gradient ($P_x = g\eta_x + \Phi_x$ is the total pressure gradient), ADV_x is the nonlinear advection term, and $(K_m u_z)_z$ represents the vertical diffusion. The momentum balance near the coastal and midshelf region of Grande Bay in EXP5 shows that the cross-shelf surface pressure gradient set up by the westerly wind peaks near the coast and decreases offshore changing sign at

Table 2. Comparison Between Observed and Modeled Time-Averaged Near-Surface Currents at Mooring Sites in the Southern Shelf Region and Shelf Break[a]

	Speed (cm s^{-1})			Angle (deg From East)		
Location	[Obs]	[Model] (EXP1)	Diff	[Obs]	[Model] (EXP1)	Diff
A (43°19′S, 63°49′W)	2.00	1.80	0.20	76	67	9
B (43°45′S, 61°31′W)	10.00	9.30	0.70	69	61	8
C (43°50′S, 59°40′W)	46.00	34.00	12.00	65	63.50	2.5
D (41°S, 57°W)	40.00	37.00	3.00	50	53	3

[a]See also Figure 7. [Obs] indicates the time-average of the observational data, [Model] indicates the average of the model results at the observational sites, and Diff indicates the magnitude of the difference between observed and computed quantities at the observational sites, shown for both the velocity magnitude difference and the angular difference. A and B observational data are taken from *Rivas* [1997]. C and D are short-term measurements taken during 2005 (51 days) and 2006 (95 days), respectively, under the Global Environmental Facility–Patagonia Project.

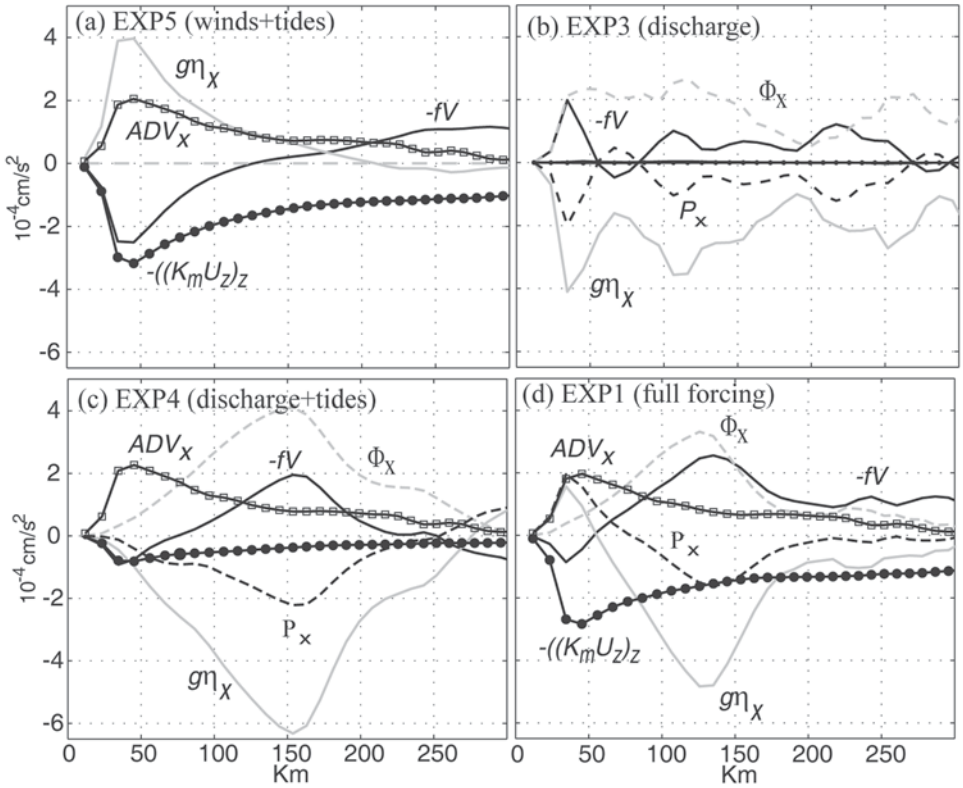

Figure 9. Cross-shore depth-integrated momentum terms in Grande Bay for (a) EXP3, (b) EXP5, (c) EXP4, and (d) EXP1. The baroclinic (Φ_x, dashed) and barotropic ($g\eta_x$, solid) pressure gradient terms are the gray lines, the total pressure gradient is the black dashed line, the Coriolis term is the black solid line, the vertical diffusion term is the line with full circles, and the advection term is the line with squares.

approximately 200 km from shore (Figure 9a). This pressure gradient generates a southward flowing current, which forms the eastern limb of the Grande Bay gyre (Figure 8a). There is no apparent signature of the middle-shelf jet in the Coriolis term. In the experiment where the shelf ocean is forced with only low-salinity discharges from the Magellan Strait (EXP3) the model predicts a reduced salinity zone that is trapped within the 20 m isobath (~50 km from the coast) and is advected northward by a relatively uniform and intense coastal current (Figure 8b). Adding the tidal forcing (EXP4) causes an offshore shift of the front, an intensification of middle-shelf jet approximately at 150 km from the coast and a weaker (southward) coastal current (Figure 9c). While the magnitude of the nonlinear advection term in this experiment is very similar to EXP5, the cross-shelf distribution of the pressure gradient is substantially modified and resembles the results of the experiment with full forcing (Figure 9d). A peak of the pressure gradient force (dominated by the surface pressure gradient) is observed near the location of the maximum along-shelf current at the front. The above analysis suggests that the modification of the cross-shelf barotropic pressure gradient produced by the interaction of the low-salinity discharge and the vigorous tidal mixing present in Grande Bay is in large part responsible for setting up the intense northward residual flow that follows the 100 m isobath. The further addition of climatological winds and the MC (EXP1) move the core of the jet inshore and slightly increases the frontal jet velocity (Figures 8d and 9d). It is important to note, however, that the influence of the MC is relatively minor because of the topographic barrier conformed by the Malvinas Islands Plateau (Figure 6b) and therefore, the region beyond 200 km offshore, like in EXP5, presents relatively uniform northward flow, mostly governed by Ekman dynamics (Figure 9d).

[21] The momentum balances indicate that the intensification of the mid- and outer-shelf circulation to the north of ~50°S (Figure 10b) is dynamically driven by the barotropic pressure gradient generated by the MC (Figures 10c and 10d). Note that in EXP5, which lacks a MC, there is a very weak mean northward current between the coast and 200 km that is driven by a pressure set-up generated by local winds (P_x) balanced by vertical mixing $(K_m u_z)_z$ (Figures 10a and 10c). In EXP1, however, the onshore extension of the negative barotropic pressure gradient generated by the MC develops a strong, geostrophically balanced, northward current, which is particularly intense north of about 47°S (Figures 10b and 10c).

[22] To end our description of the SSR circulation we will typify its seasonal variations. The stream function anomalies of the two most contrasting seasons of the benchmark experiment (EXP1) indicates a strengthening of the northward flow during the fall and a weakening during the spring (Figures 11a and 11d). The intensity of the seasonal changes is larger north of 48°S and offshore the 50 m isobath. To elucidate the cause of these variations we compared EXP1 with EXP6 and EXP2 (Table 1). EXP6 is initialized with constant density and forced by climatological wind stress.

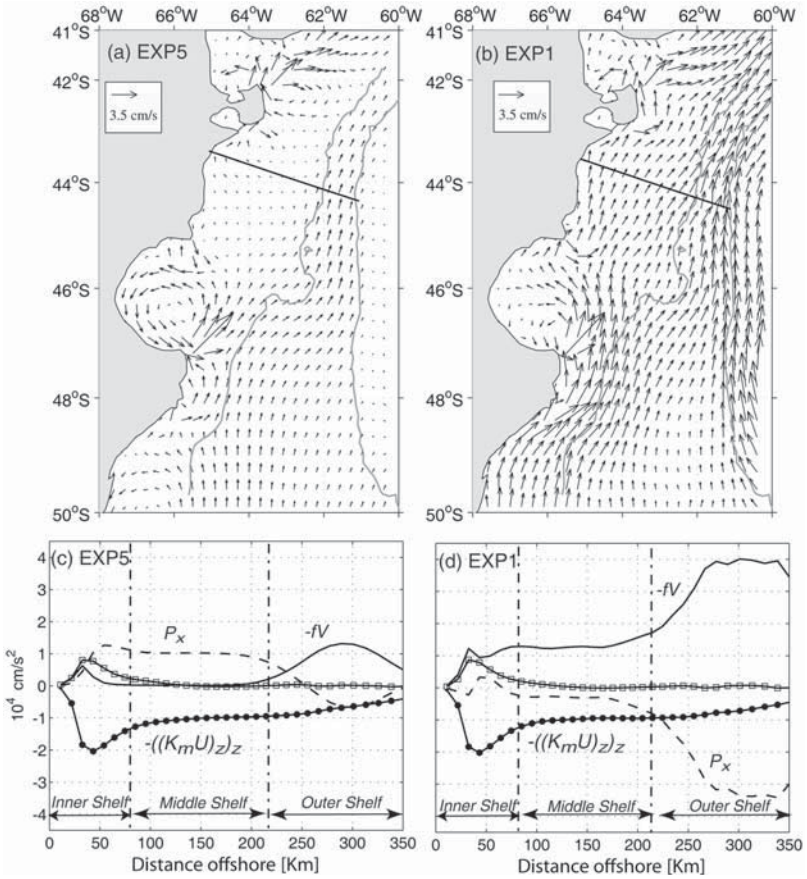

Figure 10. (a, b) Depth-averaged circulation and (c, d) cross-shore depth-integrated momentum terms in the northern SSR. Figures 10a and 10c show results from EXP5, and Figures 10b and 10d show results from EXP1. The gray lines in the Figures 10a and 10b indicate the 100 m and 200 m isobaths, and the black line indicates the cross section where the momentum terms are evaluated.

EXP2 replicates the conditions of the benchmark experiment but without tidal or wind forcing. Note that EXP1 and EXP2 incorporate, through the open boundary inflows the seasonal variations of the large-scale circulation. The comparison of these experiments indicate that the observed seasonal variations in EXP1 are driven mainly by wind forcing in the northern portion (>48°S) of the inner and middle shelf (Figures 11b and 11e), and by modulations of the MC transport in the southern region and offshore of the 100 isobath (Figures 11c and 11f). The variability of the MC transport in our model, which is derived from POCM-4C, is in agreement with observations that suggest a strengthening of the flow during the fall and weakening during the spring [*Matano et al.*, 1993; *Vivier and Provost*, 1999; *Fetter and Matano*, 2008]. The strengthening of the northward shelf transport predicted by our model during the fall and winter and weakening during the spring and summer is consistent with the diagnostic calculations of *Rivas and Langer* [1996] and *Forbes and Garraffo* [1988].

4.2.2. CSR (41°S to 28°S)

[23] The water mass structure of the CSR is shaped by the freshwater discharges from the Plata and the Patos Lagoon, and advection of Sub-Antarctic Shelf Waters from the SSR and Subtropical Shelf Waters from the NSR [*Castro and de Miranda*, 1998; *Piola et al.*, 2000]. The mean circulation in this region, particularly north of 38°S, presents marked intra-annual variations [*Piola et al.*, 2000; *Palma et al.*, 2004a], therefore we will focus our discussion on the peak months of each season. Results from the benchmark experiment shows that south of 38°S there is a general northeastward flow in the middle and outer shelf that is driven by the local wind forcing and the barotropic pressure gradient associated with the MC (Figure 12). The inner shelf is characterized by the development of an anticlockwise gyre in El Rincón Bight during the winter and its decay toward the spring and summer. This gyre did not develop in our previous barotropic simulation (spring), which instead showed a southwestward current that extended from the mouth of the La Plata River to El Rincón Bight [see *Palma et al.*, 2004a].

[24] North of 38°S the CSR shows marked seasonal variations of the circulation caused by changes in the local (winds and freshwater discharges) and remote forcing (western boundary currents). The circulation in the outer shelf, which is dominated by a poleward flow throughout the year, reflects its proximity to the BC. The circulation in the inner shelf, which is more affected by freshwater discharges and the seasonally varying winds, is directed to the northeast during the fall and early winter and to the southwest during the spring and summer (Figure 12). The

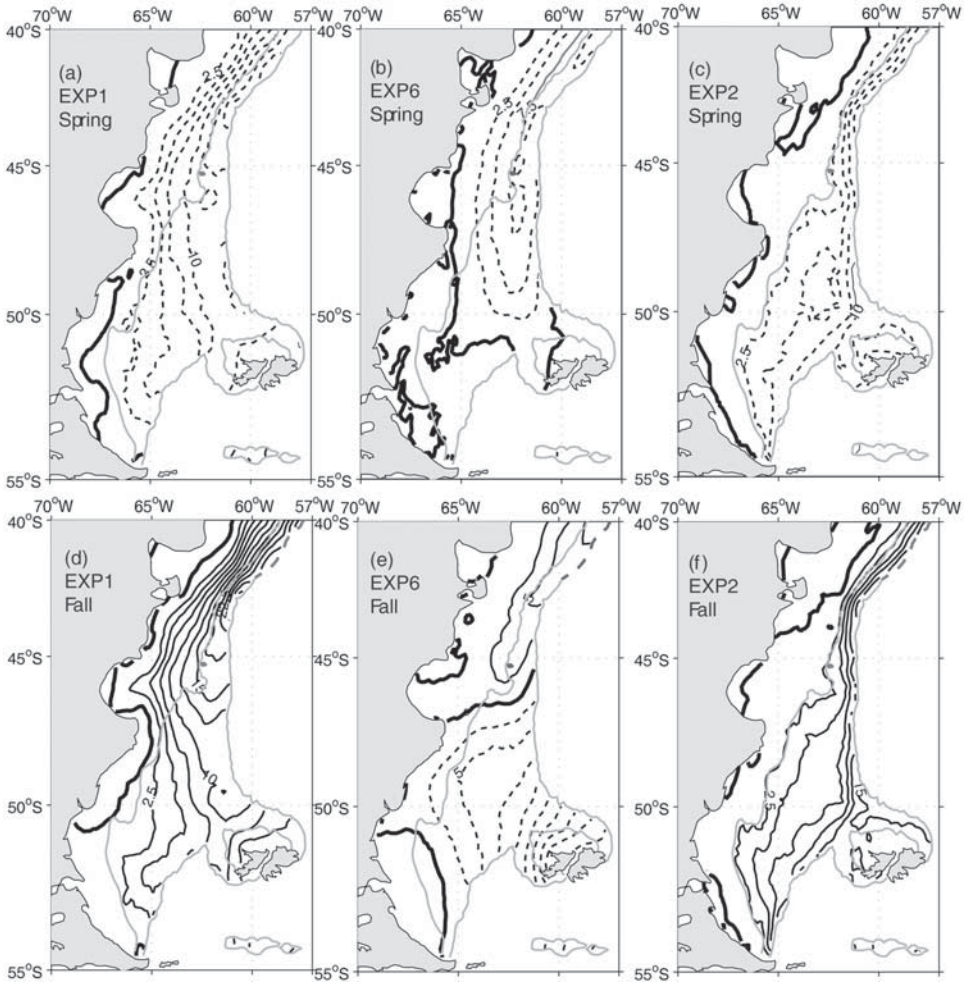

Figure 11. Transport stream function anomalies (seasonal minus annual mean) on the Southern Shelf Region. Dashed lines indicates negative anomalies, and solid lines indicate positive anomalies. (a, b, c) Spring anomalies, (d, e, f) fall anomalies. Figures 11a and 11d are results from EXP1, Figures 11b and 11e are results from EXP6, and Figures 11c and 11f are results from EXP2. The gray lines indicate the 100 m and 200 m isobaths.

circulation in the middle shelf is more variable on account of its dependence on the inner- and outer-shelf forcing and will be discussed in more detail later. Seasonal variations of these circulation patterns are clearly evidenced in the temperature and salinity fields (Figure 13). During the fall and the early winter there is a strengthening of the northeastward flow that produces intrusions of cold sub-Antarctic shelf waters and low-salinity waters from the Plata and Patos Lagoon further north (Figures 13b and 13d). During the summer the northern portion of the CSR is influenced by the onshore intrusions of the BC waters and by the retraction of the Plata plume (Figures 13a and 13c), and along the coasts of Uruguay and southern Brazil there is a development of nearshore upwelling driven by the prevailing winds (Figure 13a). Satellite observations of SST suggest that in favorable situations a large part of the Uruguayan coast ($\sim$250 km) is affected by this upwelling [*Framiñan*, 2005]. Although the seasonal variations of the La Plata discharges are relatively small its plume shows strong seasonal migrations: It drifts from approximately 38°S during the summer to 28°S during the fall, a northward excursion of more than 1200 km (Figure 13d). To further illustrate these migrations we constructed a time plot of the along-shelf evolution of the nearshore 33.5 psu isohaline, representative of the plume salinity (Figure 14a). The northern limit of the plume is located at approximately 32°30′S during the summer and moves to $\sim$27°30′S in during the early winter, following the onset of southwesterly winds during the fall, with an average expansion velocity of $\sim$145 km month^{-1}. The retreat of the plume starts during the late winter months and proceeds at a slower rate ($\sim$80 km month^{-1}), taking approximately 7 months to reach its summer location. The expansion and retraction velocity of the freshwater discharges in our simulation are in good agreement with satellite chlorophyll-a data, which are highly correlated with observed surface salinity [*Piola et al.*, 2008a] (Figure 14a). The high correlation among northward (southward) along-shelf wind stress and lower (higher) values of surface salinity depicted in coastal locations of the Southern Brazil Shelf (Figure 14b) is

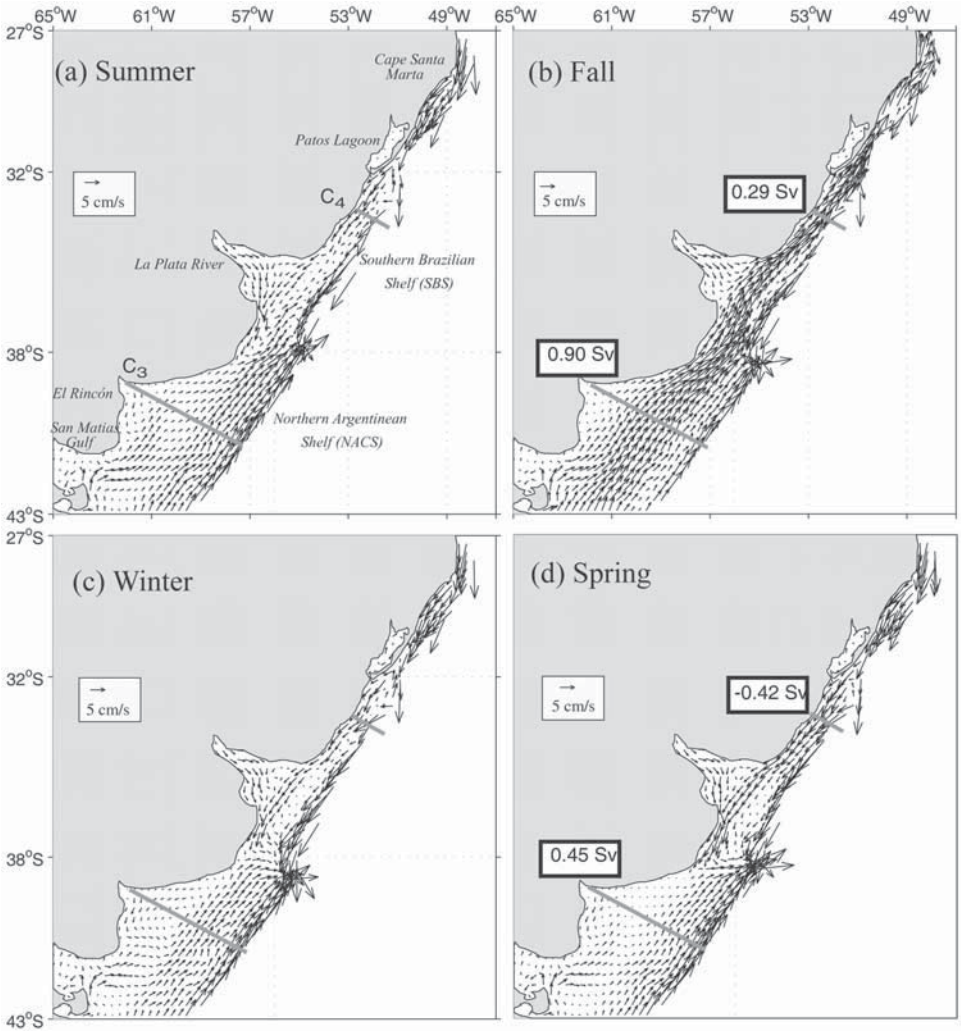

Figure 12. Depth-averaged circulation in the Central Shelf Region for (a) summer, (b) fall, (c) winter, and (d) spring. Velocity vectors greater than 0.3 m s^{-1} are not shown. The fields are shown for depths less than 500 m only. Numbers inside boxes indicate the transport (in Sv) through the indicated cross section.

indicative of the strong influence of the local wind forcing on the plume dynamics. The phase differences observed between model and observations could be attributed to errors in the phase of the wind stress used to force the model, or to the inaccuracies of the salinity-chlorophyll relation.

[25] To illustrate the vertical structure of the circulation patterns just discussed we selected representative salinity and velocity cross sections in the southern and northern portion of the CSR (C3 and C4, Figure 12a). Salinity offers the advantage of presenting relatively small seasonal variations compared to the large seasonal temperature changes. The southern region is characterized by a nearly homogeneous vertical distribution of salinity in the inner and middle shelf, and a strongly stratified shelf break front farther offshore (Figures 15a and 15b). The salinity structure of the outer shelf is very steady throughout the year but the inner shelf shows moderate seasonal variations that are controlled by intrusions of high-salinity waters ($S > 33.7$ psu) from the San Matías Gulf during the winter (Figure 15b), and by the equatorward advection of low-salinity waters ($33.5 < S < 33.7$ psu) from the SSR during the remaining seasons (Figure 15a). These changes follow the growth of the El Rincón Bight gyre during the winter months, which lead to the development of a stagnant region that allows the intrusion of high-salinity waters from the San Matias Gulf (Figures 12c and 15d). The summer collapse of the gyre and the strengthening of the middle-shelf jet facilitate the advection of fresher sub-Antarctic shelf waters from the SSR (Figures 12a and 15c). In the offshore region the most conspicuous aspect of the salinity field is the shelf break front, which is characterized by strong upwelling velocities whose intensity weakens during the winter months (Figures 15e and 15f). Although there are no direct current measurements to confirm the numerical results, the seasonal development of the El Rincón Gyre and the structure of the shelf break front and upwelling predicted by our simulation are in close agreement with the observational descriptions of *Martos and Piccolo* [1988], *Lucas et al.* [2005], and *Romero et al.* [2006]. Upwelling at the shelf break front is also indirectly suggested by the observed high levels of chlorophyll-a concentration at the

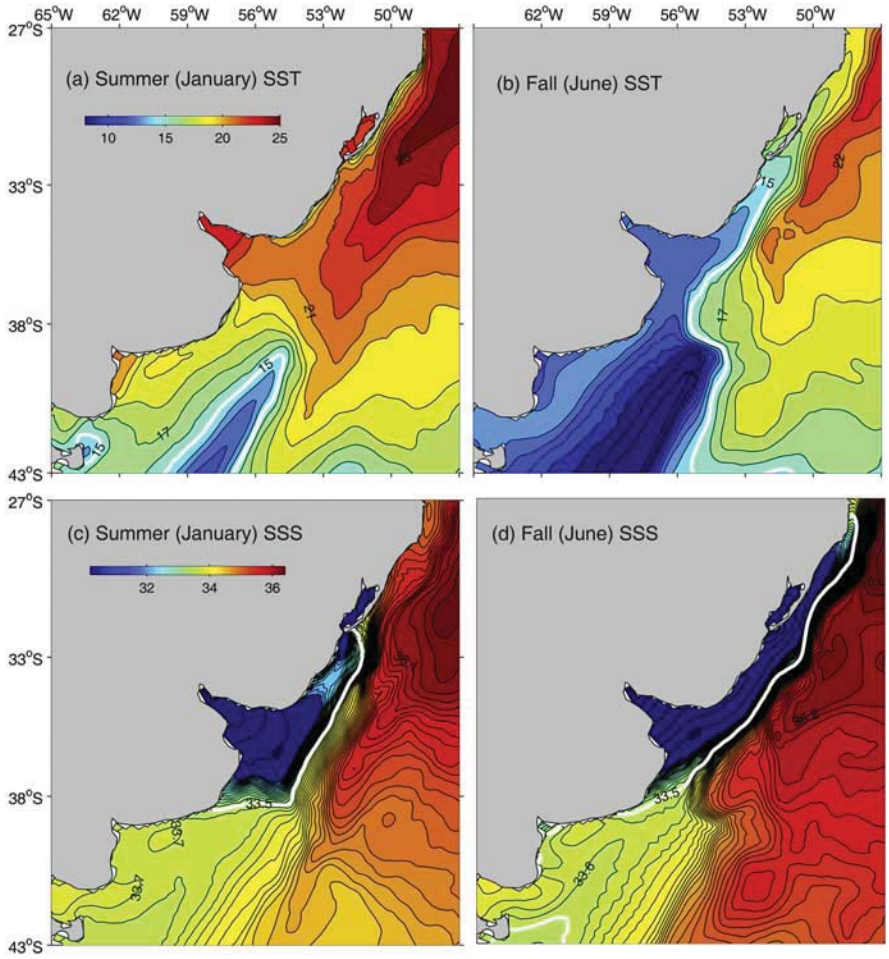

Figure 13. (a, b) Sea surface temperature (SST) and (c, d) sea surface salinity (SSS) for the CSR as obtained from the model forced by winds, tides, freshwater discharges, and offshore boundary currents (EXP1). Figures 13a and 13c are for a representative summer month (January) and Figures 13b and 13d are for a winter month (June). The white bold contours in Figures 13a and 13b indicate the 15°C isotherm, and in Figures 13c and 13d they indicate the 33.5 psu isohaline.

surface, since upwelling usually brings nutrient-rich water into the upper euphotic zone and hence facilitates primary production [*Romero et al.*, 2006].

[26] The seasonal variability of the northern portion of the CSR is dominated by the migrations of the Plata plume (Figures 16a and 16b). The largest variations occur in the inner shelf, where the northward flow reverses direction during the fall and the early winter (Figures 16c and 16d). This region has two distinct upwelling centers, one over the shelf break and the other in the nearshore area (Figures 16e and 16f). The shelf break upwelling of colder and less saline slope water occurs through the entire year. During late spring and summer southwesterly winds reinforces the intrusion of slope waters, which reach the inner shelf (Figure 16e). During the fall, however, downwelling favorable winds inhibit the entrainment of the slope waters (Figures 16b and 16f). The salinity structure generated by the model is consistent with historical data and recent synoptic surveys conducted in the area [*Castro and de Miranda*, 1998; *Piola et al.*, 2008b]. The seasonal inversion of the depth-averaged shelf circulation in the inner Southern Brazil Shelf predicted by the model have also been predicted by simplified Ekman models [*Pereira*, 1989], and observed in the analysis of hydrographic observations and wind climatologies [*Lima et al.*, 1996] and 3-D barotropic models [*Palma et al.*, 2004a].

[27] It is difficult to discriminate the relative contributions of local and remote forcing and baroclinicity on the circulation patterns just described. We will, nevertheless, attempt to assess them by comparing experiments using different model set-ups. In the southern portion of the CSR, for example, the benchmark experiment (EXP1, Table 1) shows a substantially larger along-shelf transport than the barotropic experiment forced with winds only (EXP6) [*Palma et al.*, 2004a], and a weakening of the poleward current in the inner shelf. These changes are quantified in the cross-shelf momentum balances of both experiments, which indicate that the increase of the along-shelf transport in the baroclinic experiment is generated by the barotropic cross-shelf pressure gradient set-up by the MC (Figure 17). Thus, in the southern portion of the CSR the MC is the largest contrib-

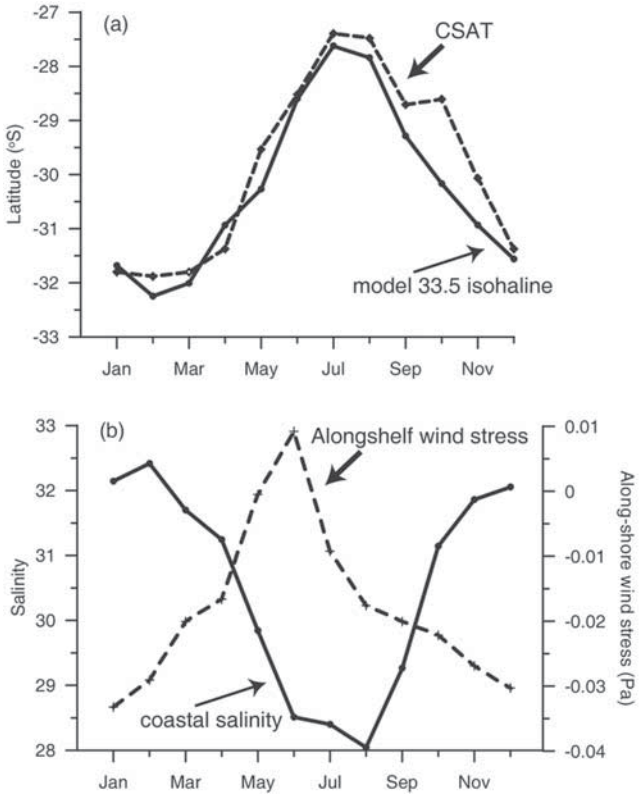

Figure 14. (a) Latitude of penetration of the model 33.5 surface isohaline (full line) and of satellite-derived chlorophyll-a (CSAT) (2.0 mg m^{-3} isoclines, dashed line) along the CSR coast (adapted from *Piola et al.* [2008a]). (b) Time evolution of the model coastal salinity (full line) and the along-shelf component of the wind stress (dashed line) near the C4 section indicated in Figure 12a.

utor to the development of the observed circulation patterns in the middle and outer shelf.

[28] To characterize the dynamical equilibrium of the northern portion of the CSR we calculated the cross-shelf momentum balances during the summer and late fall (Figure 18). These balances indicate that the along-shelf component of the circulation is dominated by a close balance between the effect of the Earth rotation and the cross-shelf pressure gradient (i.e., geostrophic balance). This relatively simple balance however, changes sign and magnitude according to the forcing and the time of the year. In EXP6, the wind forced barotropic experiment, the circulation is primarily driven by the alongshore component of the wind stress, which generates a northward flow during fall and winter, and a southward flow during spring and summer (Figures 18a and 18b (gray lines)). In EXP1, which included freshwater discharges, the downwelling favorable winds generate an intense cross-shelf salinity gradient that overcomes the negative barotropic pressure gradient set-up by the BC, and strengthens the inner- and middle-shelf jets during fall and early winter (Figure 18a (black lines)). In summer, this experiment shows the development of a northward countercurrent in the middle shelf (Figure 16c), which did not exist in the barotropic case (EXP6, Figure 18b) A similar countercurrent has been reported from observations. *Zavialov et al.* [2002] described a northward "residual" midshelf current, from short-term current meter observations, and speculated that it could be generated by the freshwater discharges. *De Souza and Robinson* [2004] using information from surface drifters deployed in the Southern Brazilian Shelf, described a northward flowing current along the 100 m isobath, and relate it to the latitudinal migrations of the Subtropical Shelf Front and the Brazil-Malvinas Confluence. We surmise that this countercurrent is driven by the cross-shelf pressure gradient generated by the MC near 38°S, which then spreads its influence in the direction of propagation of topographic shelf waves. Following *Csanady* [1978], the alongshore extent of an imposed cross-shelf surface gradient can be estimated as $L_y = fH_xW^2/r$, where H_x is the cross-shelf topographic gradient, W the cross-shelf scale of the surface gradient (set-up by the MC) and r is the bottom friction coefficient. In our particular case $H_x \sim$ 1e-3, $W \sim$ 160 km, f = 9.24 e-5, r = 0.012 and $L_y \sim$ 600 km, thus if we consider 38°S as the upper limit of the MC, the above estimate indicates that its influence should extend to ~33°S (Figure 19). Thus the model results indicate that the midshelf countercurrent of the CSR is

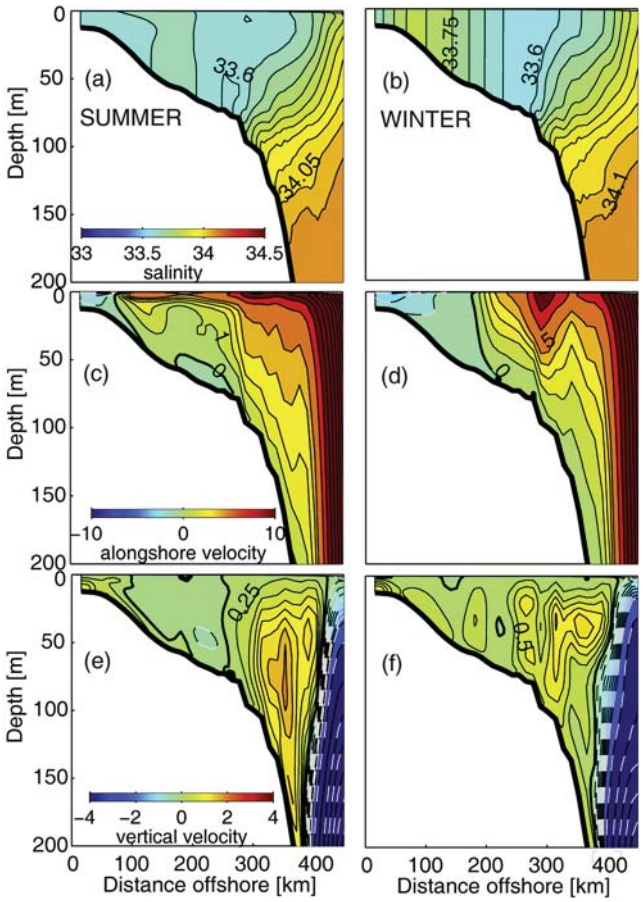

Figure 15. Cross section of (a, b) salinity, (c, d) along-shelf velocity, and (e, f) vertical velocity at the Northern Argentine Continental Shelf (NACS) (C3 in Figure 12a). Figures 15a, 15c, and 15e are for a summer month (January), and Figures 15b, 15d, and 15f are for a winter month (August).

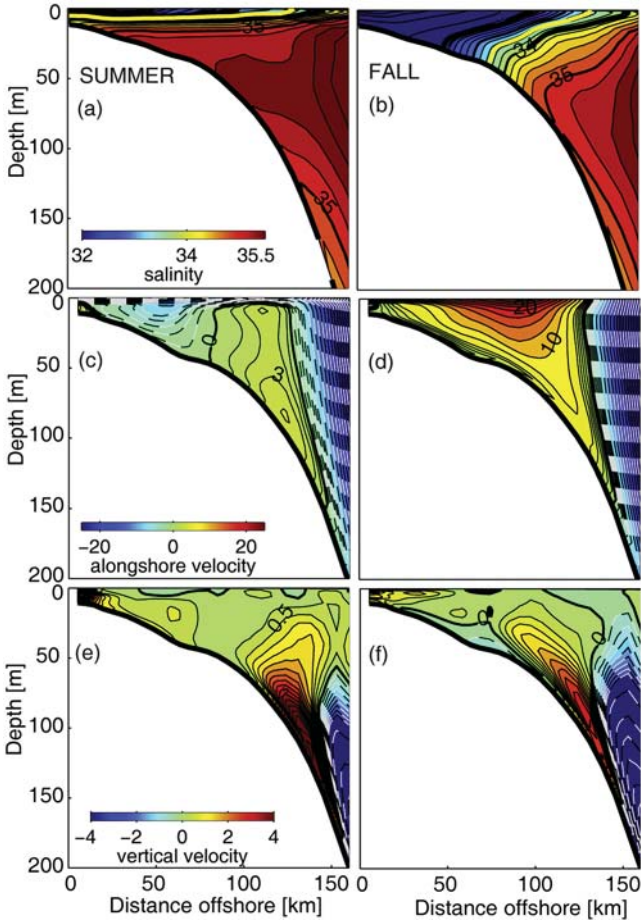

Figure 16. Cross section of (a, b) salinity, (c, d) along-shelf velocity, and (e, f) vertical velocity at the Southern Brazilian Shelf (SBS) (section C4 in Figure 12a). Figures 16a, 16c, and 16e are for a summer month (January), and Figures 16b, 16d, and 16f are for a late fall month (June).

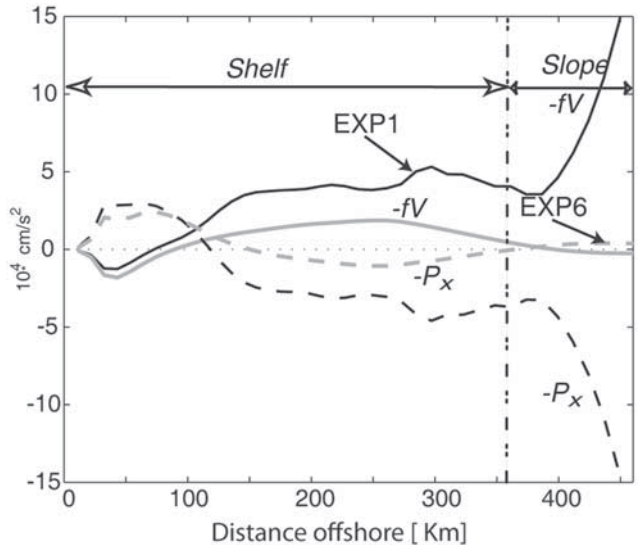

Figure 17. Comparison of the annual mean depth-averaged cross-shelf momentum balance at the NACS section (C3) of experiment EXP6 (no boundary current inflow, gray lines) and experiment EXP1 (including the MC, black lines).

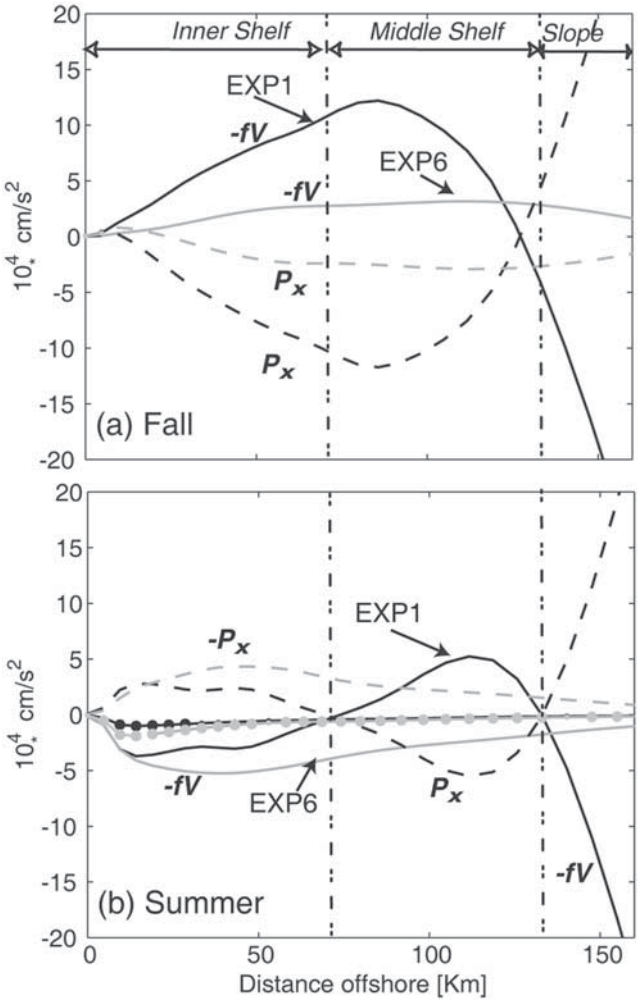

Figure 18. Comparison of the depth-averaged cross-shelf momentum balance at the SBS section (C4) of EXP6 (gray lines) and EXP1 (black lines) for (a) fall (June) and (b) summer (January).

generated by the barotropic pressure gradient associated with the MC.

[29] To investigate the generation of shelf break upwelling in the northern portion of the CSR we calculated the along-shelf momentum balance terms in the bottom boundary layer (Figure 20). The dominant balance is:

$$fu + P_y - (K_m v_\sigma)_z = 0, \quad (2)$$

where u is the cross-shore velocity, P_y is the total along-shelf pressure gradient and $(K_m v_z)_z$ is the vertical diffusion term. In EXP6 (wind forcing only) the balance shows that the pressure gradient and the vertical friction terms have pronounced presence in the inner and middle shelf and tend to balance each other (Figures 20a and 20c). There is a very weak boundary layer cross-shelf flow in the outer shelf that reverses seasonally. In EXP1 however, this balance indicates that near the shelf break, the along-shelf pressure gradient associated with the BC drives an upslope current ($fu > 0$) (and hence upwelling) in the bottom boundary layer (Figures 20b and 20d). During the fall the vertical mixing

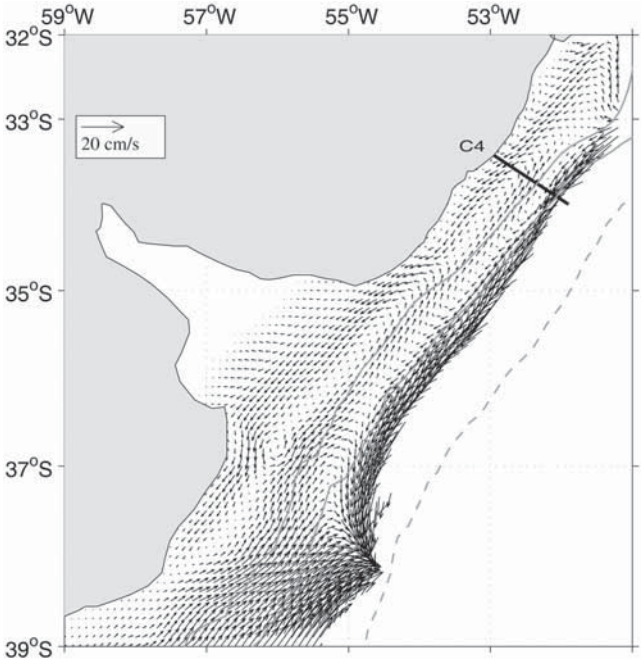

Figure 19. Near-surface (15 m) summer mean currents from EXP1. The modeled vector field has been interpolated onto a regular grid for presentation. The 100 m and 200 m isobaths (solid gray curves), the 1000 m isobath (dashed line), and the SBS cross section (C4) are included. Vectors outside the 500 m isobath are not shown. Note the offshore Brazil-Malvinas Confluence near 38°S and the continuous northward shelf current from this point up to 33°S closely following the 100 m isobath.

reinforces the upslope flow in the outer shelf and slope but *opposes* the inshore flow in the middle and inner shelf (Figure 20b). During the summer the along-shelf pressure gradient increases in the middle shelf and the bottom friction term changes sign in the inner shelf (Figure 20d). While the increase in the pressure gradient seems to be related to variations in the BC intensity, the change of sign of the vertical mixing term in the inner shelf (inshore the 60 m isobath) appears to be driven by the seasonal changes of the wind direction (Figures 20b and 20d). Both effects *reinforce* the up-shelf flow of slope waters from the shelf break toward the coast and promote the appearance of a cold SST strip along the Southern Brazilian Shelf coastline during summer (Figure 13a).

4.2.3. NSR (28°S to 22°S)

[30] This region is characterized by low-amplitude tides, predominantly northeasterly (alongshore) winds and the poleward flow of the Brazil Current near the shelf's edge. There are no significant freshwater inputs in this area, although observations indicate that there are intrusions of the Plata plume into the southern portion of this region, particularly during the fall and winter seasons [*Castro and de Miranda*, 1998; *Piola et al.*, 2000]. The circulation in the NSR is dominated by the local wind forcing in the inner shelf and is highly influenced by the BC in the middle and outer shelf [*Campos et al.*, 1995; *Castro and de Miranda*, 1998; *Castelao et al.*, 2004].

[31] The model results show marked seasonal changes in the NSR circulation, particularly in the middle and inner shelf, which are caused by the seasonal variations of the atmospheric forcing (Figure 21). During the late spring and summer (not shown) there is a sharp SST front, located at ~60 km from the coast, in the northern half of the bight that

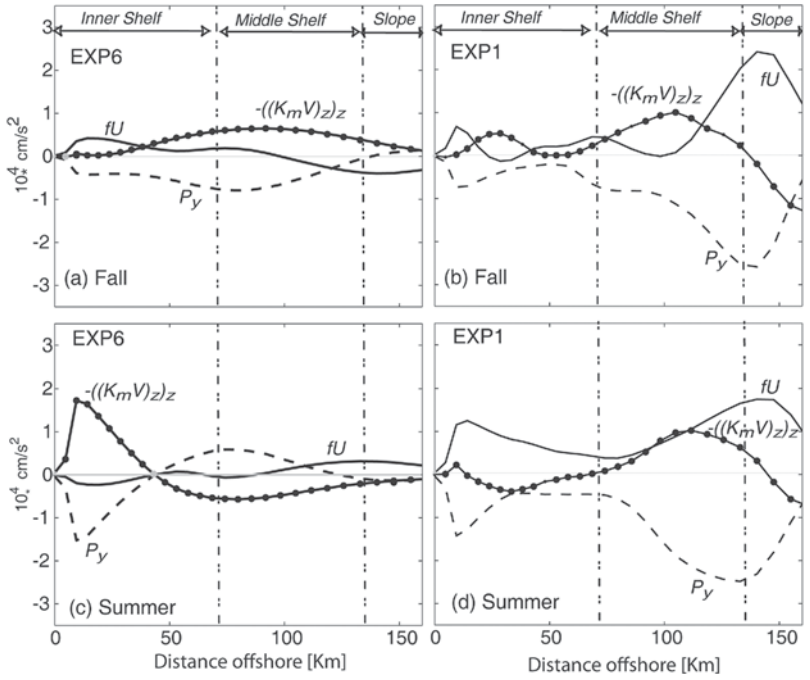

Figure 20. Comparison of the bottom boundary layer along-shelf momentum balance at the SBS section (C4) of the experiments EXP6 (gray lines) and EXP1 (black lines) for (a, b) a late fall month (June) and (c, d) a summer month (January).

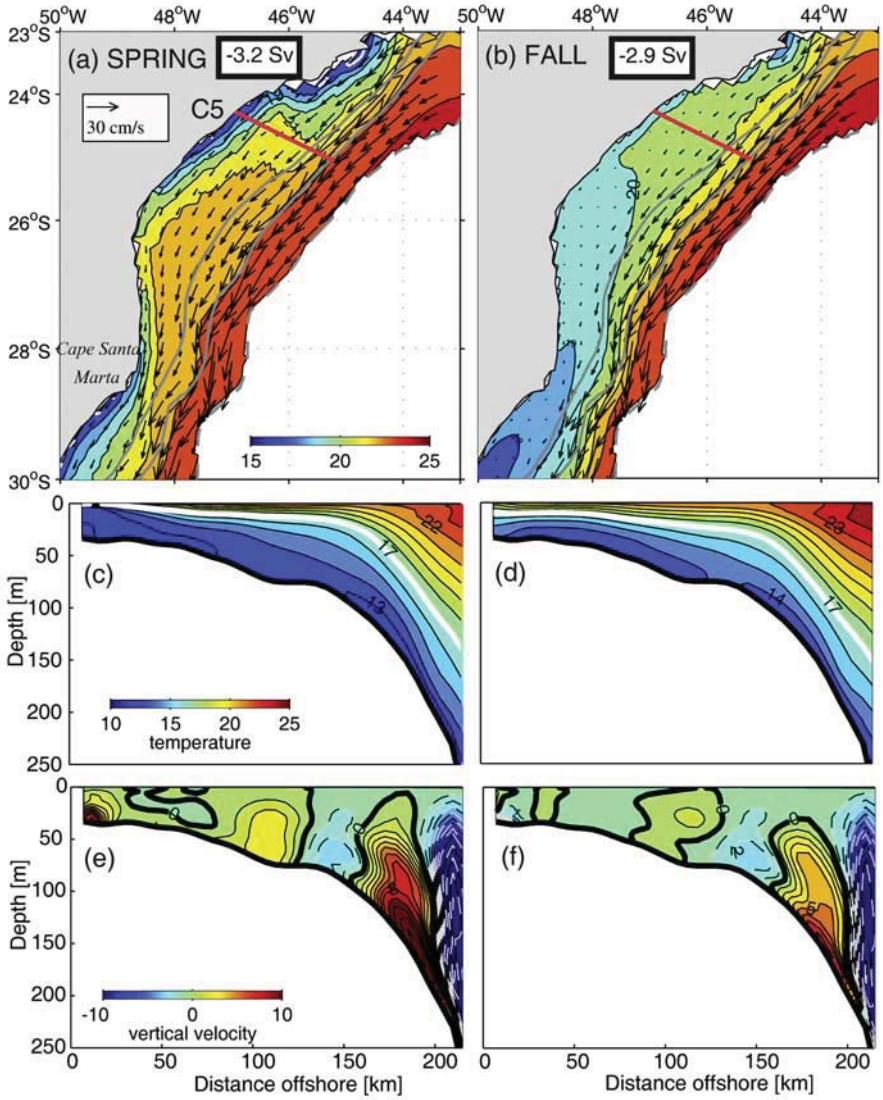

Figure 21. (a, b) Sea surface temperature (background color) and depth-averaged velocity vectors in the Northern Shelf Region (EXP1). Numbers inside boxes indicate the transport (in Sv) through the cross section. (c, d) Cross sections of temperature and (e, f) cross sections of vertical velocity component. Figures 21a, 21c, and 21e are from late spring (November), and Figures 21b, 21d, and 21f are from late fall (June). Note that the temperature scale is different for the horizontal and vertical sections. In Figures 21a and 21b, gray lines indicate the 100 m and 200 m isobaths, and the red lines indicate the cross section of Figures 21c, 21d, 21e, and 21f) (C5).

separates the warm and salty tropical waters of the deep ocean from the colder (T < 20°C) coastal waters (Figure 21a). The depth-averaged circulation pattern consists of a southwestward flow with a mean speed of 0.1 m s^{-1} in the inner shelf and 0.4 m s^{-1} in the outer shelf. These patterns are consistent with the observations described by *Castro and de Miranda* [1998]. There is a marked weakening of the offshore SST gradients on the shelf during the fall and winter (Figure 21b). The cold SST tongue in the southwestern portion of the bight evidences the penetration of southern waters, which follow the strengthening of the northward flow from the CSR and the simultaneous weakening of the local northeasterly winds. Additional cooling of the shelf waters during the winter, leads to the formation of a SST front near the shelf break. A comparison of the along-shelf transports in this simulation with EXP6 shows a threefold increase of the along-shelf transport due the barotropic pressure gradient associated with the offshore flow of the BC (Figure 21). Analysis of satellite-derived SST data south of 30°S reveals similar seasonal changes in the shelf break SST gradients [*Saraceno et al.*, 2004].

[32] The most conspicuous feature of the thermal structure of the NSR is the cold SST tongue in the nearshore region (Figure 21a). This tongue reflects the interplay between the inner and the shelf break upwelling regimes (Figures 21e and 21f). The former is driven by the local winds and the later by the BC, which pumps cold and low-salinity South Atlantic Central Waters onto the outer shelf (T < 20°C) (Figures 21c and 21d). Upwelling favorable winds further entrain these waters onto the shelf and to the

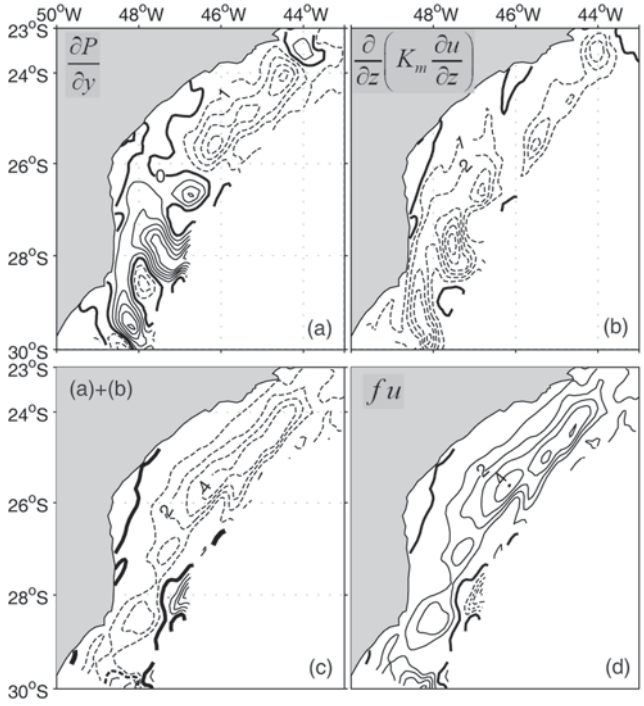

Figure 22. Horizontal distribution of the steady state bottom boundary layer along-shelf momentum balance in the NSR from EXP2. (a) Along-shelf pressure gradient, (b) vertical friction, (c) sum of Figures 22a and 22b, and (d) Coriolis term. Note that positive *fu* indicates onshore flow.

surface. The shelf break upwelling is a continuous phenomena but the coastal upwelling, which is closely tied to the seasonal cycles of the alongshore wind stress, peaks during the spring and summer and weakens considerably during the fall and winter (Figures 21e and 21f).

[33] To quantify the dynamical mechanisms that generate the shelf break upwelling we computed the bottom boundary layer along-shelf momentum balance in EXP2, which replicates the benchmark experiment without wind forcing (Figure 22 and Table 1). The magnitude of the along-shelf pressure gradient (P_y), which is of the same order as the Coriolis force and the vertical friction terms, indicates that the along-shelf changes in orientation of the coastline and the bottom topography contribute significantly to the development of the observed upwelling patterns. Without this effect the dominant balance would have been a classical Ekman bottom boundary layer balance i.e., vertical mixing balancing Coriolis. The indentation of the coastline, however, allows the development of along-shelf pressure gradients that change the circulation in the bottom boundary layer. The widening and narrowing of the shelf, for example, leads to the development of a reversal of direction of the along-shelf pressure gradient, and hence to larger onshore shelf break velocities in the north than in the south (Figures 22a and 22d). This balance, therefore, indicates that in the north the upslope flow is driven by alongshore pressure gradients with a smaller contribution of vertical diffusion while in the south it is primarily driven by vertical diffusion and regulated by the adverse action of the pressure gradient (Figures 22a and 22b). Once the colder water has been entrained onto the shelf upwelling winds could drive them farther up onto the water column. This balance is similar to that described by *Oke and Middleton* [2000] off Eastern Australia although they did not discussed the effect of variable alongshore pressure gradients in the bottom boundary layer.

[34] In previous analyses *Campos et al.* [2000] and *Castelao et al.* [2004] speculated that shelf break upwelling in this region is a sporadic process associated with the passage of meanders of the Brazil Current. Our results, however, indicate that shelf break upwelling is a persistent feature of the regional circulation (e.g., Figure 21e). In spite of the observed differences it should be noted that the upwelling mechanism proposed by *Campos et al.* [2000] and *Castelao et al.* [2004] and that proposed herein are not mutually exclusive but, in fact, they reinforce each other. However, while the presence of meanders and eddies near the shelf break is a sporadic, though quite frequent phenomena, our results indicate that the sole existence of a steady poleward slope current in the presence of variable along-shelf topography can lead to a persistent upslope flow. *Castro and de Miranda* [1998] ascribed the presence of cold waters in the northern bight during summer to the advection of cold water located farther north (Cape Frío region). Our analysis shows that a portion of cold slope waters may be brought to the coast locally by the combined action of offshore forcing and wind-induced upwelling.

5. Summary and Conclusions

[35] In this study we analyzed the SWAS circulation employing a set of three dimensional numerical simulations. The benchmark experiment includes tides, winds, freshwater discharges and offshore western boundary currents. Additional experiments varying the initialization and forcing fields were designed to explain the contribution made by various processes in driving the mean shelf circulation and its seasonal variability. Although historical observations of currents are too sparse and too short to construct climatological estimates of the circulation to compare with the model results, there is a general agreement with previous observations and simplified regional models [*Castro and de Miranda*, 1998; *Romero et al.*, 2006; *Piola et al.*, 2000, 2008a, 2008b; *Forbes and Garraffo*, 1988; *Rivas and Langer*, 1996; *Pereira*, 1989; *Castelao et al.*, 2004] indicating that the primary physical processes are well represented in the model.

[36] The present solutions also reveal important additional features of the shelf circulation not previously reported. According to our results the annual mean circulation in the south of the SSR has an average northeastward transport of ~0.7 Sv, and it is characterized by the formation of a distinct jet, known as the Patagonian Current, which is generated by the combined effects of the low-salinity discharges from Magellan Straits, tidal mixing, and the wind stress forcing (Figure 8d). The Malvinas Islands, near the shelf break region, buffers the shelf circulation from the effects of the deep ocean circulation. North of ~50°S, however, the cross-shelf barotropic pressure gradient generated by the MC strongly influences the shelf circulation. There is a strengthening of the northward transport during

the fall and a weakening during the spring. These seasonal variations are driven by the wind forcing in the inner and middle shelf, and the MC in the outer shelf (Figure 11).

[37] The CSR circulation shows a general southward flow in the outer shelf and a northward flow in the middle shelf. The inner-shelf region shows strong seasonal changes, which are followed by significant anomalies of the temperature and salinity fields. During fall and early winter the thermal structure is modulated by waters advected northward from the SSR and La Plata (Figures 13b and 13d). During summer there is advection from the BC and local upwelling (Figures 13a and 13c). The high correlation between along-shelf wind stress and surface salinity in coastal locations of the SBS demonstrates the strong influence of local wind stress over the Plata plume (Figure 14b). The general circulation in the NSR is dominated by a general southwestward flow that weakens during the fall. The SST patterns of this region show large seasonal changes that follow the interaction between the locally wind driven circulation and the BC (Figure 21).

[38] One of the main conclusions of this study is that the neighboring western boundary currents have a very important effect on the shelf circulation. The most evident of which is the increase of along-shelf transport in EXP1 as compared to those reported in our previous study (EXP5 and EXP6) [*Palma et al.*, 2004a]. There are more subtle dynamical influences such as the development of a northward middle shelf current in the CSR that, during summer, flows against the predominantly northwesterly winds. Although the existence of this current has been confirmed by observations its origin was originally ascribed to freshwater influences [*Zavialov et al.*, 2002] or seasonal migrations of the Subtropical Shelf Front [*de Souza and Robinson*, 2004]. Our model results, however, indicate that this current is generated by the upstream spreading (in the arrested topographic wave sense) of pressure gradients set-up farther south by the MC. Thus, our analysis shows that the influence of the MC extends several degrees north of its confluence point (Figure 19).

[39] The influence of western boundary currents on the adjacent continental shelves is a common feature among various regions of the world ocean [*Loder et al.*, 1998a]. Representative works that analyze these interactions in open shelves regions include those of *Boicourt et al.* [1998] for the Gulf Stream–South Atlantic Bight shelf, *Loder et al.* [1998b] for the Gulf Stream–Labrador Current–Middle Atlantic Bight, *Weisberg and Hue* [2003] for the Gulf of Mexico Loop Current–West Florida Shelf, and *Roughan and Middleton* [2002] for the East Australian Current–New South Wales shelf in Australia. There are some similarities between these regions and the interaction of the boundary currents with the SWAS described in this paper, but also distinct differences. Topographically induced meandering of the Gulf Stream are believed to be a source of upwelling to the shelf in the South Atlantic Bight [*Osgood et al.*, 1987] and previous studies demonstrated similar influences of the BC on the NSR. For example, *Campos et al.* [2000] and *Castelao et al.* [2004] ascribed the observed shelf break upwelling of SACW in the NSR to the passage of meanders and eddies produced by instabilities of the BC. Our analysis, however indicates that upwelling in the NSR is a persistent feature of the shelf break region driven by changes in the mean path of the BC caused by along-shelf topographic variations. This mechanism is supported by the analysis of the along-shelf momentum balance in the bottom boundary layer which shows that in regions where the BC turns inshore the along-shelf pressure gradient generates a geostrophic onshore current that uplifts slope water onto the shelf (Figure 22). The analysis is similar to that described by *Oke and Middleton* [2000] off Eastern Australia although they ascribed the upwelling to enhanced bottom friction induced by nonlinear dynamics rather than variable alongshore pressure gradients in the bottom boundary layer. The further entrainment of slope waters onto the nearshore region depends on the local wind forcing. For example, during upwelling favorable seasons (spring-summer) the shores of the Uruguay, southern Brazil and northern NSR are marked by a coastal strip of colder waters (Figures 13a and 21a) previously intruded onto the shelf via shelf break upwelling mechanisms described above.

[40] The observed chlorophyll blooms of the MC [*Romero et al.*, 2006] are symptomatic of the upwelling of nutrient-rich waters to the surface (Figures 14e and 14f), but the mechanisms that may drive such upwelling are still under debate. Previous studies, particularly in the Middle Atlantic Bight [i.e., *Gawarkiewicz and Chapman*, 1992; *Pickart*, 2000] have shown that the internal processes associated with the formation of shelf break fronts in regions dominated by cyclonic currents can also generate shelf break upwelling. On account of the physical differences between the two regions however, it is unclear whether the same theories can be applied to the SSR. In a recent article *Matano and Palma* [2008] proposed that the shelf break upwelling in the SSR (Figures 15e and 15f) is associated with the spreading of the boundary current (i.e., MC) onto the shelf, which generates a diverging horizontal velocity field that is compensated by upwelling from below. In the proposed model the shelf break dynamics are not controlled by the downslope buoyancy flux generated by a shelf current, as postulated by previous authors for the Middle Atlantic Bight, but by the meridional pressure gradient generated by the slope current.

[41] **Acknowledgments.** Support for E. D. Palma and A. R. Piola came from Agencia Nacional de Promoción Científica y Tecnológica (ANCYPT-grant PICT04–25533), CONICET (grant PIP04–6138) and by Collaborative Research Network grant CRN2076 from the Inter-American Institute for Global Change Research, supported by the U.S. National Science Foundation grant GEO-0452325. E.D.P. acknowledges partial support by Universidad Nacional del Sur (grant F032). R. Matano was supported by NASA grant NAG512378, JPL Contract 1206714, and NSF grant OCE-0726994. This paper benefited substantially from comments and suggestions given by the anonymous reviewers. The authors would like to thank Michael Schlax for kindly providing us the satellite data used in Figure 3.

References

Acha, M., H. Mianzan, R. Guerrero, M. Favero, and J. Bava (2004), Marine fronts at the continental shelves of austral South America, Physical and ecological processes, *J. Mar. Syst.*, *44*, 83–105, doi:10.1016/j.jmarsys.2003.09.005.

Bianchi, A. A., L. Bianucci, A. R. Piola, D. Ruiz Pino, I. Schloss, A. R. Poisson, and C. F. Balestrini (2005), Vertical stratification and air-sea CO_2 fluxes in the Patagonian shelf, *J. Geophys. Res.*, *110*, C07003, doi:10.1029/2004JC002488.

Bisbal, G. A. (1995), The Southeast South American shelf large marine ecosystem: Evolution and components, *Mar. Policy*, *19*(1), 21–38, doi:10.1016/0308-597X(95)92570-W.

Blumberg, A. F., and G. L. Mellor (1987), A description of a three-dimensional coastal ocean circulation model, in *Three Dimensional Coastal Ocean*

Models, *Coastal Estuarine Sci.*, vol. 4, edited by N. Heaps, pp. 1–16, AGU, Washington, D. C.

Boicourt, W. C., W. J. Wiseman Jr., A. Valle-Levinson, and L. P. Atkinson (1998), Continental shelf of the southeastern United States and the Gulf of Mexico in the shadow of the western boundary current, in *The Sea*, vol. 11, edited by A. R. Robinson and K. H. Brink, pp. 135–182, John Wiley, New York.

Brandhorst, W., and J. P. Castello (1971), Evaluación de los recursos de anchoíta (*Engraulis Anchoita*) frente a la Argentina y Uruguay. I. Las condiciones oceanográficas, sinopsis del conocimiento actual sobre la anchoíta y el plan para su evaluación, *Ser. Informes Tec. 29*, 63 pp, Proyecto de Desarrollo Pesquero, Mar del Plata, Argentina.

Campos, E. J., J. Goncalves, and Y. Ikeda (1995), Water mass characteristics and geostrophic circulation in the South Brazil Bight: Summer of 1991, *J. Geophys. Res.*, *100*, 18,537–18,550, doi:10.1029/95JC01724.

Campos, E. J., D. Velhote, and I. C. da Silveira (2000), Shelf break upwelling driven by Brazil Current cyclonic meanders, *Geophys. Res. Lett.*, *27*(6), 751–754, doi:10.1029/1999GL010502.

Casey, K. S., and P. Cornillon (1999), A comparison of satellite and in situ based sea surface temperature climatologies, *J. Clim.*, *12*, 1848–1863, doi:10.1175/1520-0442(1999)012<1848:ACOSAI>2.0.CO;2.

Castelao, R. M., E. J. D. Campos, and J. L. Miller (2004), A modelling study of coastal upwelling driven by wind and meanders of the Brazil Current, *J. Coastal Res.*, *20*(3), 662–671, doi:10.2112/1551-5036(2004)20[662:AMSOCU]2.0.CO;2.

Castro, B. M., and L. B. de Miranda (1998), Physical oceanography of the western Atlantic continental shelf located between 4°N and 34°S, in *The Sea*, *11*, vol. 11, edited by A. R. Robinson and K. H. Brink, pp. 209–251, John Wiley, New York.

Costanza, R., et al. (1997), The value of the world's ecosystem services and natural capital, *Nature*, *387*, 253–280, doi:10.1038/387253a0.

Csanady, G. T. (1978), The arrested topographic wave, *J. Phys. Oceanogr.*, *8*, 47–62, doi:10.1175/1520-0485(1978)008<0047:TATW>2.0.CO;2.

de Souza, R. B., and I. S. Robinson (2004), Lagrangian and satellite observations of the Brazil Coastal Current, *Cont. Shelf Res.*, *24*, 241–262, doi:10.1016/j.csr.2003.10.001.

Egbert, G. D., A. F. Bennet, and M. G. Foreman (1994), TOPEX/POSEIDON tides estimated using a global inverse model, *J. Geophys. Res.*, *99*, 24,821–24,852, doi:10.1029/94JC01894.

Fetter, A. F. H., and R. P. Matano (2008), On the origins of the variability of the Malvinas Current in a global, eddy-permitting numerical simulation, *J. Geophys. Res.*, doi:10.1029/2008JC004875, in press.

Forbes, M. C., and Z. D. Garraffo (1988), A note on the mean seasonal transport on the Argentinean shelf, *J. Geophys. Res.*, *93*, 2311–2319, doi:10.1029/JC093iC03p02311.

Framiñan, M. B. (2005), On the physics, circulation and exchange processes of the Río de la Plata estuary and the adjacent shelf, Ph.D. dissertation, Rosenstiel Sch. of Mar. and Atmos. Sci., 486 pp., Univ. of Miami, Miami, Fla.

Garzoli, S. L., and C. Giulivi (1994), What forces the variability of the southwestern Atlantic boundary currents?, *Deep Sea Res., Part I*, *41*, 1527–1550, doi:10.1016/0967-0637(94)90059-0.

Gawarkiewicz, G., and D. C. Chapman (1992), The role of stratification in the formation and maintenance of shelfbreak fronts, *J. Phys. Oceanogr.*, *22*, 753–772, doi:10.1175/1520-0485(1992)022<0753:TROSIT>2.0.CO;2.

Glorioso, P. D., and R. A. Flather (1995), A barotropic model of the currents off SE South America, *J. Geophys. Res.*, *100*, 13,427–13,440, doi:10.1029/95JC00942.

Glorioso, P. D., and R. A. Flather (1997), The Patagonian Shelf tides, *Prog. Oceanogr.*, *40*, 263–283, doi:10.1016/S0079-6611(98)00004-4.

Gordon, A. L., and C. L. Greengrove (1986), Geostrophic circulation of the Brazil-Falkland Confluence, *Deep Sea Res., Part A*, *33*, 573–585, doi:10.1016/0198-0149(86)90054-3.

Greenberg, D. A., J. W. Loder, Y. Shen, D. R. Lynch, and C. E. Naimie (1997), Spatial and temporal structure of the barotropic response of the Scotian Shelf and Gulf of Maine to surface wind stress: A model-based study, *J. Geophys. Res.*, *102*, 20,897–20,915, doi:10.1029/97JC00442.

Guerrero, R. A., and A. R. Piola (1997), Masas de agua en la plataforma continental, in *El Mar Argentino y Sus Recursos Pesqueros*, vol. 1, pp. 107–118, Inst. Nac. de Invest. y Desarrolla Pesquero, Mar del Plata, Argentina.

Harari, J., and R. de Camargo (2003), Numerical simulation of the tidal propagation in the coastal region of Santos (Brazil), 24°S 46°W, *Cont. Shelf Res.*, *23*, 1597–1613, doi:10.1016/S0278-4343(03)00143-2.

Levitus, S., and T. P. Boyer (1994), *World Ocean Atlas 1994*, vol. 4, *Temperature*, *NOAA Atlas NESDIS*, vol. 4, 129 pp., NOAA, Silver Spring, Md.

Levitus, S., R. Burgett, and T. P. Boyer (1994), *World Ocean Atlas 1994*, vol. 3, *Salinity*, *NOAA Atlas NESDIS*, vol. 3, 111 pp., NOAA, Silver Spring, Md.

Lima, I. D., C. A. E. Garcia, and O. Moller (1996), Ocean surface processes on the Southern Brazilian Shelf: Characterization and seasonal variability, *Cont. Shelf Res.*, *16*, 1307–1317.

Loder, J. B., W. C. Boicourt, and J. H. Simpson (1998a), Western ocean boundary shelves coastal segment (W), in *The Sea*, vol. 11, edited by A. R. Robinson and K. H. Brink, pp. 3–27, John Wiley, New York.

Loder, J. B., B. Petrie, and G. Gawarkiewicz (1998b), Physical oceanography of the western Atlantic continental shelf located between 4°N and 34°S, in *The Sea*, vol. 11, edited by A. R. Robinson and K. H. Brink, pp. 209–251, John Wiley, New York.

Lucas, A. J., R. A. Guerrero, H. W. Mianzán, M. E. Acha, and C. A. Lasta (2005), Coastal oceanographic regimes of the Northern Argentine Continental Shelf (34–43°S), *Estuarine Coastal Shelf Sci.*, *65*, 405–420, doi:10.1016/j.ecss.2005.06.015.

Martos, P., and M. C. Piccolo (1988), Hydrography of the Argentine Continental Shelf between 38° and 42°S, *Cont. Shelf Res.*, *8*, 1043–1056, doi:10.1016/0278-4343(88)90038-6.

Matano, R. P. (1993), On the separation of the Brazil Current from the coast, *J. Phys. Oceanogr.*, *23*, 79–90, doi:10.1175/1520-0485(1993)023<0079:OTSOTB>2.0.CO;2.

Matano, R. P., and E. D. Palma (2008), On the upwelling of downwelling currents, *J. Phys. Oceanogr.*, doi:10.1175/2008JPO3783.1, in press.

Matano, R. P., M. G. Schlax, and D. B. Chelton (1993), Seasonal variability in the southwestern Atlantic, *J. Geophys. Res.*, *98*, 18,027–18,035, doi:10.1029/93JC01602.

Oke, P. R., and J. H. Middleton (2000), Topographically induced upwelling off eastern Australia, *J. Phys. Oceanogr.*, *30*, 512–531, doi:10.1175/1520-0485(2000)030<0512:TIUOEA>2.0.CO;2.

Olson, D. B., G. P. Podesta, R. H. Evans, and O. Brown (1988), Temporal variations in the separation of the Brazil and Malvinas currents, *Deep Sea Res., Part A*, *35*, 1971–1990, doi:10.1016/0198-0149(88)90120-3.

Osgood, K. E., J. M. Bane, and W. K. Dewar (1987), Vertical velocities and dynamical balances in Gulf Stream meanders, *J. Geophys. Res.*, *92*, 13,029–13,040, doi:10.1029/JC092iC12p13029.

Palma, E. D., and R. P. Matano (2000), On the implementation of open boundary conditions to a general circulation model: The 3-D case, *J. Geophys. Res.*, *105*, 8605–8627, doi:10.1029/1999JC900317.

Palma, E. D., R. P. Matano, and A. R. Piola (2004a), A numerical study of the Southwestern Atlantic Shelf circulation: Barotropic response to tidal and wind forcing, *J. Geophys. Res.*, *109*, C08014, doi:10.1029/2004JC002315.

Palma, E. D., R. P. Matano, A. R. Piola, and L. Sitz (2004b), A comparison of the circulation patterns over the Southwestern Atlantic Shelf driven by different wind stress climatologies, *Geophys. Res. Lett.*, *31*, L24303, doi:10.1029/2004GL021068.

Panella, S., A. Michelato, R. Perdicaro, G. Magazzú, F. Decembrini, and P. Scarazzato (1991), A preliminary contribution to the understanding of the hydrological characteristics of the Strait of Magellan: Austral spring 1989, *Bolletino Oceanol. Teor. Appl.*, *9*(2–3), 107.

Pereira, C. S. (1989), Seasonal variability in the coastal circulation on the Brazilian continental shelf (29°S–35°S), *Cont. Shelf Res.*, *9*, 285–299, doi:10.1016/0278-4343(89)90029-0.

Peterson, R. G. (1992), The boundary current in the western Argentine Basin, *Deep Sea Res., Part A*, *39*, 623–644, doi:10.1016/0198-0149(92)90092-8.

Peterson, R. G., and L. Stramma (1991), Upper-level circulation in the South Atlantic Ocean, *Prog. Oceanogr.*, *26*, 1–73, doi:10.1016/0079-6611(91)90006-8.

Peterson, R. G., C. S. Johnson, W. Krauss, and R. E. Davies (1996), Lagrangian measurements in the Malvinas Current, in *The South Atlantic: Present and Past Circulation*, edited by G. Wefer et al., pp. 239–247, Springer, New York.

Pickart, R. S. (2000), Bottom boundary layer structure and detachment in the shelfbreak jet of the Middle Atlantic Bight, *J. Phys. Oceanogr.*, *30*, 2668–2686, doi:10.1175/1520-0485(2001)031<2668:BBLSAD>2.0.CO;2.

Piola, A. R., and R. P. Matano (2001), The South Atlantic Western Boundary Currents Brazil/Falkland (Malvinas) Currents, in *Encyclopedia of Ocean Sciences*, vol. 1, edited by J. M. Steele, S. A. Thorpe, and K. K. Turekian, pp. 340–349, Elsevier, New York.

Piola, A. R., E. J. D. Campos, O. O. Moller, M. Charo, and C. Martinez (2000), Subtropical shelf front off eastern South America, *J. Geophys. Res.*, *105*, 6565–6578, doi:10.1029/1999JC000300.

Piola, A. R., R. P. Matano, E. D. Palma, O. O. Möller, and E. J. D. Campos (2005), The influence of the Plata River discharge on the western South Atlantic shelf, *Geophys. Res. Lett.*, *32*, L01603, doi:10.1029/2004GL021638.

Piola, A. R., S. I. Romero, and U. Zajaczkovski (2008a), Space-time variability of the Plata plume inferred from ocean color, *Cont. Shelf Res.*, *28*, 1556–1567, doi:10.1016/j.csr.2007.02.013.

Piola, A. R., O. O. Moller, R. A. Guerrero, and E. D. Campos (2008b), Variability of the Subtropical Shelf Front off eastern South America: Winter 2003 and summer 2004, *Cont. Shelf Res.*, *28*, 1639–1648, doi:10.1016/j.csr.2008.03.013.

Rivas, A. L. (1994), Spatial variation of the annual cycle of temperature in the Patagonian shelf between 40° and 50° of south latitude, *Cont. Shelf Res.*, *14*, 1539–1554.

Rivas, A. L. (1997), Current meter observations in the Argentine Continental Shelf, *Cont. Shelf Res.*, *17*, 391–406, doi:10.1016/S0278-4343(96)00039-8.

Rivas, A. L., and A. F. Langer (1996), Mass and heat transport in the Argentine Continental Shelf, *Cont. Shelf Res.*, *16*, 1283–1285, doi:10.1016/0278-4343(95)00063-1.

Romero, S. L., A. R. Piola, M. Charo, and C. E. García (2006), Chlorophyll-a variability off Patagonia based on SeaWiFS data, *J. Geophys. Res.*, *111*, C05021, doi:10.1029/2005JC003244.

Roughan, M., and J. H. Middleton (2002), A comparison of observed upwelling mechanisms off the east coast of Australia, *Cont. Shelf Res.*, *22*, 2551–2572, doi:10.1016/S0278-4343(02)00101-2.

Saraceno, M., C. Provost, A. R. Piola, J. Bava, and A. Gagliardini (2004), Brazil Malvinas Frontal System as seen from 9 years of advanced very high resolution radiometer data, *J. Geophys. Res.*, *109*, C05027, doi:10.1029/2003JC002127.

Saunders, P. M., and B. A. King (1995), Bottom currents derived from a shipborne ADCP on WOCE cruise A11, *J. Phys. Oceanogr.*, *25*, 329–347, doi:10.1175/1520-0485(1995)025<0329:BCDFAS>2.0.CO;2.

Smith, R. D., and D. T. Sandwell (1997), Global sea floor topography from satellite altimetry and ship depth soundings, *Science*, *277*, 1956–1962, doi:10.1126/science.277.5334.1956.

Stramma, A. L. (1989), The Brazil Current transport south of 23°S, *Deep Sea Res., Part A*, *36*, 639–646.

Tokmakian, R., and P. Challenor (1999), On the joint estimation of model and satellite sea surface height anomaly errors, *Ocean Modell. 1*, pp. 39–52, Hooke Inst. Oxford Univ., Oxford, U. K.

Trenberth, K. E., W. G. Large, and J. G. Olson (1990), The mean annual cycle in global wind stress, *J. Phys. Oceanogr.*, *20*, 1742–1760, doi:10.1175/1520-0485(1990)020<1742:TMACIG>2.0.CO;2.

Vigan, X., C. Provost, and G. Podesta (2000), Sea surface velocities from sea surface temperature image sequences 2. Application to the Brazil-Malvinas Confluence area, *J. Geophys. Res.*, *105*, 19,515–19,534, doi:10.1029/2000JC900028.

Vivier, F., and C. Provost (1999), Direct velocity measurements in the Malvinas Current, *J. Geophys. Res.*, *104*, 21,083–21,103, doi:10.1029/1999JC900163.

Weisberg, R. H., and R. Hue (2003), Local and deep-ocean forcing contributions to anomalous water properties on the West Florida Shelf, *J. Geophys. Res.*, *108*(C6), 3184, doi:10.1029/2002JC001407.

Zavialov, P. O., I. Wainer, and J. M. Absy (1999), Sea surface temperature variability off southern Brazil and Uruguay as revealed from historical data since 1854, *J. Geophys. Res.*, *104*, 21,021–21,032.

Zavialov, P. O., O. O. Möller Jr., and E. J. D. Campos (2002), First direct measurements of currents on the continental shelf of southern Brazil, *Cont. Shelf Res.*, *22*, 1975–1986, doi:10.1016/S0278-4343(02)00049-3.

R. P. Matano, College of Oceanic and Atmospheric Sciences, Oregon State University, Corvallis, OR 97331, USA.

E. D. Palma, Departamento de Física, Universidad Nacional del Sur, Bahia Blanca 8000, Argentina. (uspalma@criba.edu.ar)

A. R. Piola, Departamento Oceanografía, Servicio de Hidrografía Naval, Buenos Aires 1271, Argentina.